Limnol. Oceanogr., 57(4), 2012, 989–1010

doi:10.4319/lo.2012.57.4.0989

Basin-scale inputs of cobalt, iron, and manganese from the Benguela-Angola front to the South Atlantic Ocean

Abigail E. Noble,[a,b,1] Carl H. Lamborg,[a] Dan C. Ohnemus,[a,b] Phoebe J. Lam,[a] Tyler J. Goepfert,[a,b] Chris I. Measures,[c] Caitlin H. Frame,[a,b] Karen L. Casciotti,[a] Giacomo R. DiTullio,[d] Joe Jennings,[e] and Mak A. Saito [a,*]

[a] Department of Marine Chemistry and Geochemistry, Woods Hole Oceanographic Institution, Woods Hole, Massachusetts
[b] Massachusetts Institute of Technology-Woods Hole Oceanographic Institution Joint Program in Chemical Oceanography, Department of Marine Chemistry and Geochemistry, Woods Hole Oceanographic Institution, Woods Hole, Massachusetts
[c] Department of Oceanography, University of Hawaii, Honolulu, Hawaii
[d] Department of Biology, College of Charleston, Charleston, South Carolina
[e] College of Oceanic & Atmospheric Sciences, Oregon State University, Corvallis, Oregon

Abstract

We present full-depth zonal sections of total dissolved cobalt, iron, manganese, and labile cobalt from the South Atlantic Ocean. A basin-scale plume from the African coast appeared to be a major source of dissolved metals to this region, with high cobalt concentrations in the oxygen minimum zone of the Angola Dome and extending 2500 km into the subtropical gyre. Metal concentrations were elevated along the coastal shelf, likely due to reductive dissolution and resuspension of particulate matter. Linear relationships between cobalt, N_2O, and O_2, as well as low surface aluminum supported a coastal rather than atmospheric cobalt source. Lateral advection coupled with upwelling, biological uptake, and remineralization delivered these metals to the basin, as evident in two zonal transects with distinct physical processes that exhibited different metal distributions. Scavenging rates within the coastal plume differed for the three metals; iron was removed fastest, manganese removal was 2.5 times slower, and cobalt scavenging could not be discerned from water mass mixing. Because scavenging, biological utilization, and export constantly deplete the oceanic inventories of these three hybrid-type metals, point sources of the scale observed here likely serve as vital drivers of their oceanic cycles. Manganese concentrations were elevated in surface waters across the basin, likely due to coupled redox processes acting to concentrate the dissolved species there. These observations of basin-scale hybrid metal plumes combined with the recent projections of expanding oxygen minimum zones suggest a potential mechanism for effects on ocean primary production and nitrogen fixation via increases in trace metal source inputs.

Cobalt, iron, and manganese play essential roles as micronutrients in ocean ecosystems. These metals are involved in photosynthesis, nitrogen fixation, and many other cellular processes (Morel et al. 2003), but can exist in such low concentrations in seawater that they may limit or co-limit the growth of primary producers in the open ocean (Moore and Braucher 2008; Saito et al. 2008). Iron is predicted to limit 40% of ocean productivity and much of the marine nitrogen fixation capacity (Moore et al. 2009). Photosystems I and II (PSI and PSII) are iron intensive, and iron is required in many enzymatic pathways of the microbial nitrogen loop, including nitrogen fixation (Morel et al. 2003; Saito et al. 2011). Manganese, while typically abundant in the upper ocean of tropical and subtropical waters, is used to oxidize water to O_2 in PSII, to detoxify cells from harmful O_2^- radicals via its incorporation into superoxide dismutase, and it is an electron acceptor for manganese-oxidizing bacteria (Tebo et al. 1984; Moffett and Ho 1996; Morel et al. 2003). Cobalt has been demonstrated to co-limit the growth of some phytoplankton in culture studies (Saito and Goepfert 2008), and some field studies either as inorganic cobalt (Saito et al. 2005) or as the metallocenter of vitamin B_{12} in high-latitude environments (Bertrand et al. 2007; Panzeca et al. 2008). Cobalt can also be incorporated into the active site of carbonic anhydrase in diatoms (Morel et al. 2003), and is required by the abundant marine cyanobacteria *Prochlorococcus* and *Synechococcus* (Sunda and Huntsman 1995; Saito et al. 2002).

Recent decades of field sampling and careful, low-level analyses have identified sources and sinks to the water column trace metal inventory that include aeolian deposition, hydrothermal venting, riverine discharge, anthropogenic-derived input, reductive dissolution, sediment resuspension, biological uptake and remineralization, and scavenging (Bruland and Lohan 2003). With these observations, dissolved metal profiles have been categorized into conservative, nutrient-like, scavenged, and hybrid-type (Bruland and Lohan 2003). Iron, cobalt, and manganese fall into the hybrid-type category since their distributions are controlled by a combination of phytoplankton uptake, which creates nutrient-like distributions in the photic zone, and scavenging, which creates scavenged-like distributions in intermediate and deep waters. These three metals are distinct from other trace element micronutrients, such as zinc and nickel, because they are redox active, and have small oceanic inventories and whole-ocean residence times on the order of 40–150 yr due to scavenging (Bruland et al. 1994; Saito and Moffett 2002). Scavenging

*Corresponding author: mak@whoi.edu

[1]Present address: Department of Earth, Atmospheric and Planetary Sciences, Massachusetts Institute of Technology, Cambridge, Massachusetts

plays an important role in preventing accumulation of hybrid-type metals with thermohaline circulation, which is seen in the accumulation of macronutrients like phosphate and nitrate, and nutrient-type trace metals like cadmium and zinc between ocean basins. The reduced forms of these hybrid-type metals can be introduced to oxygenated seawater by reductive dissolution within anoxic pore waters (Heggie and Lewis 1984), exchange with particles (Lam et al. 2006; Lohan and Bruland 2008), organic matter decomposition, and photoreduction (Sunda and Huntsman 1988), while scavenging removes them from the water column. The biotic oxidation of manganese and cobalt by manganese-oxidizing bacteria is thought to be an important removal mechanism for these two metals (Tebo et al. 1984; Moffett and Ho 1996). Complexation by organic ligands is thought to protect iron and cobalt from scavenging to some degree (Johnson et al. 1997; Saito and Moffett 2001), and recent work has suggested that manganese may also be complexed by some marine siderophores (Parker et al. 2007), although the influence of complexation on manganese scavenging is still largely unknown.

A primary goal of this study was to investigate how the relative distributions of cobalt, iron, and manganese change across a strong biogeochemical gradient found in the oxygen minimum zone (OMZ) of the South Atlantic Ocean. This was accomplished by collection and analysis of a full-depth zonal cross section of these dissolved metals during the Cobalt, Iron, and Microorganisms from the Upwelling to the Gyre (CoFeMUG) cruise in November 2007. The South Atlantic Ocean is understudied with respect to trace metals (Moore et al. 2009), and understanding the biogeochemical cycling of metals near the Angola Dome and Benguela Upwelling is of economic interest to due to the presence of a major fishery. An OMZ extends from the coast, generated by a combination of high productivity and poor ventilation (Lass and Mohrholz 2008; Mohrholz et al. 2008), and this redox gradient likely affects hybrid-type metal distributions. The South Atlantic has also been presumed to not be subject to iron limitation due to its low macronutrient abundances and aeolian input; however, the lower limit of iron concentrations during the low dust season had not previously been investigated in detail. The cruise track was chosen to cross the oligotrophic gyre and penetrate the Benguela Upwelling during a period of high upwelling and low dust deposition. We present evidence of significant sources of metals to the South Atlantic Basin from the African coast and discuss their biological interactions and relative removal rates.

Methods

Sampling techniques—The CoFeMUG cruise aboard the R/V *Knorr* (16 November–13 December 2007; Chief Scientist, Saito) employed a trace metal sampling program for three transects in the South Atlantic Ocean. The main transect crossed the basin from west to east, beginning at 11°S, 330°E, and ending at 14.75°S, 12.2°E (Figs. 1, 2). This transect consisted of 19 stations that were sampled to 800 m or to near bottom in profiles of 11 or 22 depths, respectively. Shallow and deep casts alternated at a 2.5-degree longitudinal spacing. This was followed by a short, north-to-south coastal transect (Sta. 20–23) and a short, east-to-west southern transect at 25°S (Sta. 23–27, Figs. 1, 2). Acid-cleaned, Teflon-coated X-Niskin sampling bottles (OceanTest Equipment) of 8-liter capacity were deployed on an epoxy-coated rosette (Sea-Bird Electronics) attached to a nonmetallic line and were programmed to trip at predetermined depths and record sampling depths.

All bottles used to store seawater prior to analysis were soaked overnight in the acidic detergent Citranox, rinsed thoroughly with Milli-Q water (Millipore), filled with 10% HCl to soak for 10 d, rinsed thoroughly with Milli-Q water adjusted to pH 2, and double-bagged. Low-density polyethylene bottles were used for trace metal sample storage and high-density polyethylene bottles were used for nutrient sample storage. Immediately following collection, the X-Niskins were pressurized with 99.999% N_2, and seawater was filtered through Teflon tubing and a 142-mm, 0.4-μm polycarbonate plastic sandwich filter (Geotech Environmental Equipment) into sample storage bottles in a positive pressure class-100 clean environment. All tubing and filters were acid-washed prior to use. Samples intended for dissolved iron and manganese analyses were acidified to pH 1.7 with high-purity HCl (Seastar) within 6 months of sampling, and stored acidified at room temperature for at least 8 months prior to analysis. Samples intended for all cobalt analyses were not acidified and were kept at 4°C in darkness until analysis.

Cobalt analyses—Concentrations of total dissolved and labile cobalt were determined using a previously described cathodic stripping voltammetry (CSV) method (Saito and Moffett 2001; Saito et al. 2004) both during the cruise and upon returning to the laboratory. Measurements were made using the Eco-Chemie μAutolab-III systems connected to Metrohm 663 VA Stands equipped with hanging mercury drop electrodes and Teflon sampling cups. Standard additions were carried out with Metrohm 765 Dosimats using a programmed dosing procedure (Noble et al. 2008).

For total dissolved cobalt analyses, samples were ultraviolet (UV) irradiated for 1 h prior to analysis using a Metrohm 705 UV digester to degrade the organic ligands that bind cobalt and allow binding by the added electroactive cobalt ligand, dimethylglyoxime. Samples were analyzed in 8.5-mL aliquots with the addition of 30 μL recrystalized dimethylglyoxime (DMG; 0.1 mol L^{-1} in methanol), 1.5 mL purified sodium nitrite (1.5 mol L^{-1} in Milli-Q water), and 50 μL purified *N*-(2-hydroxyethyl)piperazine-*N*-(3-propanesulfonic acid) (EPPS) buffer (0.5 mol L^{-1} in Milli-Q water) (*see* Saito and Moffett 2001 for cleanup protocols). Analysis began with a 180-s purge with 99.999% N_2. Each sample was conditioned at −0.6 V for 90 s at a stir rate of 2500 revolutions per minute (rpm) followed by a 10-s equilibration step and a linear sweep from −0.6 V to –1.4 V at a rate of 10 V s^{-1}. Cobalt concentrations were determined by the standard additions technique, with initial concentrations measured in triplicate followed by four 25 pmol L^{-1} cobalt additions.

While the precision of this method using a single set of reagents is excellent (e.g., mean and standard deviation of triplicate analyses of a surface-water sample = 32 ± 0.7 pmol L^{-1}), careful analysis of reagent blanks is a crucial component of the cobalt method, and presented a new challenge for application to the analysis of an ocean section. The analytical blank was determined by analyzing seawater that had been UV irradiated for 1 h, equilibrated overnight with prepared Chelex-100 resin beads (Bio-Rad), and UV irradiated a second time to degrade any leached synthetic ligands. Blanks for each batch of reagent (nitrite, DMG, EPPS) were subtracted from the initial sample concentration. During the cruise, two batches of reagents were contaminated as observed by both an abrupt and systematic increase in sample concentrations at Sta. 13 and 15 relative to adjacent profiles and by confirmation by reanalysis of the reagent blank while at sea. Upon returning to the lab, the systematic offsets for these samples were again confirmed using two independent techniques: reanalysis in the lab by CSV, and analysis by inductively coupled plasma–mass spectrometry (ICP-MS). This in-lab CSV reanalysis of seven profiles (114 samples), performed with one set of reagents with a blank of 6 ± 1.7 pmol L^{-1} (n = 19), quantified the contamination of the reagents as an average offset of 28 and 47 pmol L^{-1} relative to the pre-contaminated blanks (both 6 pmol L^{-1}), and was consistent with the at-sea reanalysis of the blank (where the offset was determined by the average difference between the at-sea and in-lab analyses for a given reagent batch). However, an additional artifact was uncovered by this comparison of at-sea to in-lab analyses: data points in the 100–500-m OMZ range (five data points per profile) were found to have a signal loss of cobalt during reanalysis, potentially due to oxidation or precipitation in the sample bottles with time and were excluded from the offset calculation (Noble and Saito in prep.). The averaged blank concentrations for the seven reagent batches used in this data set were 4 ± 1.9 pmol L^{-1} (n = 4), 6 ± 1.7 pmol L^{-1} (n = 19), 7 ± 1.7 pmol L^{-1} (n = 4), 7 ± 1.7 pmol L^{-1} (n = 4), 8 ± 0.9 pmol L^{-1} (n = 3), 28 ± 1.4 pmol L^{-1} (n = 4), and 49 ± 6.6 pmol L^{-1} (n = 2). Twelve stations were analyzed 15 months after sampling (4, 6, 8, 10, 12, 14, 16, 23, 24, 25, 26, 27). Of those stations, 10, 12, 14, and 16 have been excluded from the data set presented here because samples appeared to have experienced some loss of cobalt with time within the OMZ described above (< 100 μmol O_2 kg^{-1}), which was apparent by comparison to adjacent profiles that were measured at sea. In contrast, Sta. 4, 6, and 8 (found outside the OMZ) were oceanographically consistent with adjacent profiles that were analyzed at sea, and have been included, as well as Sta. 23–27. With the exception of two data points from Sta. 23 and four data points from Sta. 24, the in-lab analyses from these stations were from waters with oxygen concentrations above 100 μmol kg^{-1}. Additionally, good reproducibility between shipboard and shore-based determinations was observed previously for samples from the well-oxygenated Ross Sea > 17 months after sampling. In this case the shore-based recovery was 97% ± 12% relative to the at sea values (n = 9, A. E. Noble and M. A. Saito unpubl.). This suggests that non-OMZ samples can be successfully preserved by this storage technique. In future studies, care should be taken to minimize the number of reagent batches used to avoid systematic errors, to carefully constrain and minimize the cobalt reagent blank, and to continually monitor for small but important systematic error caused by contamination.

For labile cobalt analyses, 8.5 mL of filtered sample was added to clean Teflon vials preconditioned with a small aliquot of sample water. Thirty microliters of DMG was added to each vial and allowed to equilibrate overnight in the dark (Saito et al. 2004). Analyses were then performed as described for total concentrations with the addition of the remaining two reagents and use of the standard addition technique. Previously, we determined that natural cobalt ligands in seawater have conditional stability constants of > $10^{16.8}$ (Saito et al. 2005), suggesting that the cobalt is bound very tightly to the cobalt ligands. Thus, we define labile cobalt as the fraction of total dissolved cobalt that is either bound to weak organic and inorganic ligands in seawater or present as free Co(II), and is then exchangeable with the complexing agent (DMG) used for analysis (Saito et al. 2004, 2005). The difference between the total dissolved cobalt and the labile cobalt can then be used as an estimation of the strong cobalt ligand concentration. Three sets of reagents were used for these analyses, with blanks of 4 ± 1.9 pmol L^{-1} (n = 4), 5 ± 0.7 pmol L^{-1} (n = 3), and 7 ± 1.7 pmol L^{-1} (n = 4).

At the time of this expedition, low-level total seawater cobalt intercalibration data were not yet available. In recent years, our lab has participated in the GEOTRACES Intercalibration effort (www.geotraces.org), which, upon our urging, examined and documented the importance of UV oxidation for total cobalt analysis, and our results are presented in Table 1 (Bruland 2010).

Iron and manganese analyses—Total dissolved iron and manganese were measured using ICP-MS, as described by Saito and Schneider (2006). Briefly, 13.0-mL aliquots of acidified seawater were weighed into cleaned polypropylene centrifuge tubes and ^{57}Fe was added for isotope dilution analysis and equilibrated overnight. Concentrated ammonium hydroxide (Seastar) was added to induce $Mg(OH)_2$ and trace metal coprecipitation for 3 min, followed by centrifugation for 3 min at 3000 rpm (1460 × g) using an Eppendorf Centrifuge 5810R. The supernatant was decanted, the sample was centrifuged and decanted again, and the pellet was dissolved in 5% nitric acid (Seastar) containing 1 μg L^{-1} indium. The 5% nitric acid resuspension solution was used to estimate the ^{56}Fe, ^{57}Fe, and ^{55}Mn reagent and instrument blank, and signal suppression due to matrix effects was accounted for by using a ratio of the indium in the blank to the indium in the resuspended sample solution, as described in Saito and Schneider (2006). The Sampling and Analysis of Fe (SAFe) seawater intercalibration standards were analyzed at the beginning of each analysis day with iron concentrations of 0.96 ± 0.095 nmol L^{-1} for the D2 seawater standard and 0.125 ± 0.046 nmol L^{-1} for the S1 seawater standard (n = 10), which are within the reported ranges of 0.91 ± 0.17 nmol L^{-1} and 0.097 ± 0.043 nmol L^{-1} (Johnson et al. 2007).

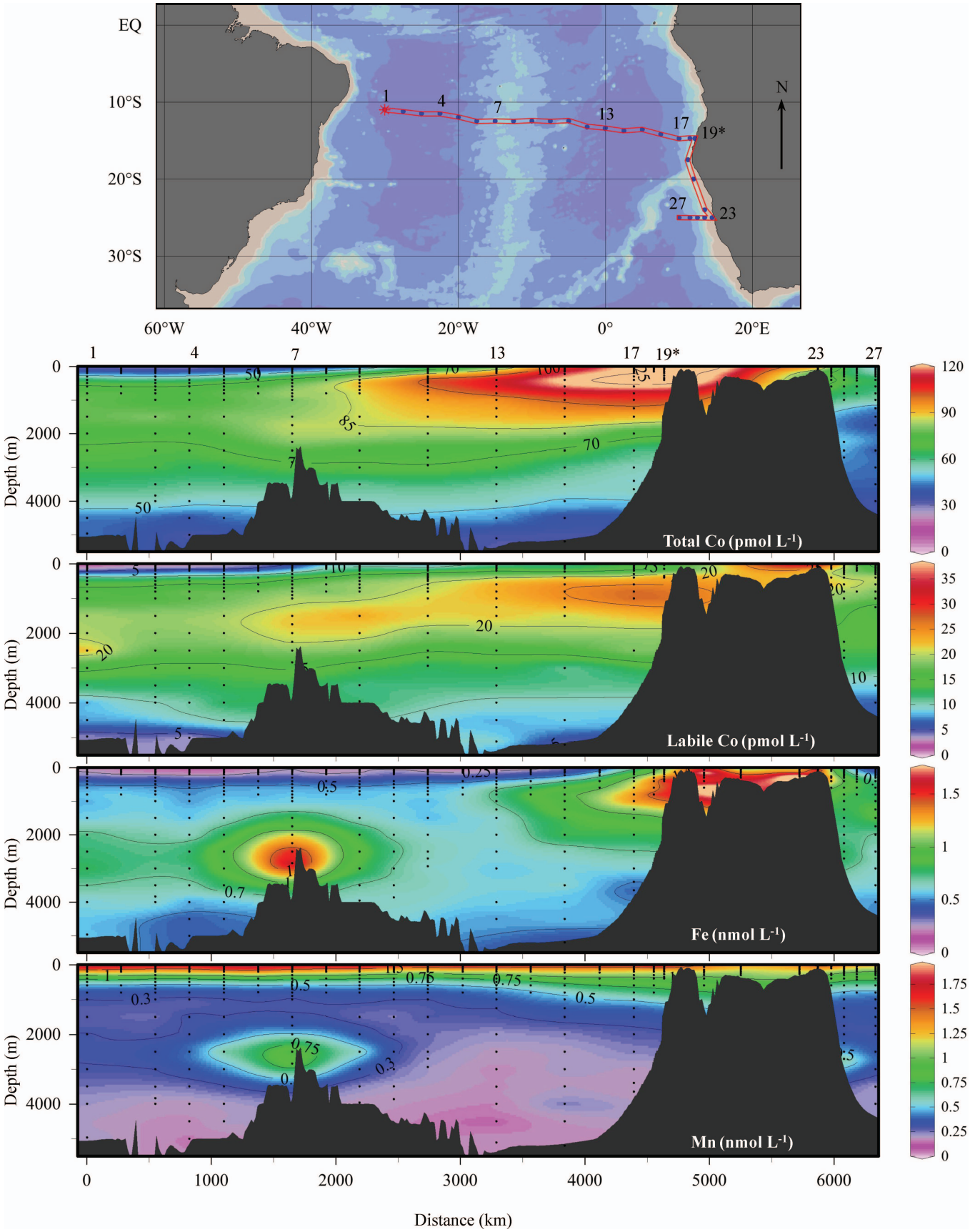
EQ
10°S
20°S
30°S
60°W
40°W
20°W
0°
20°E
N
1
4
7
13
17
19*
23
27
Depth (m)
Total Co (pmol L-1)
Labile Co (pmol L-1)
Fe (nmol L-1)
Mn (nmol L-1)
Distance (km)
0
1000
2000
3000
4000
5000
6000

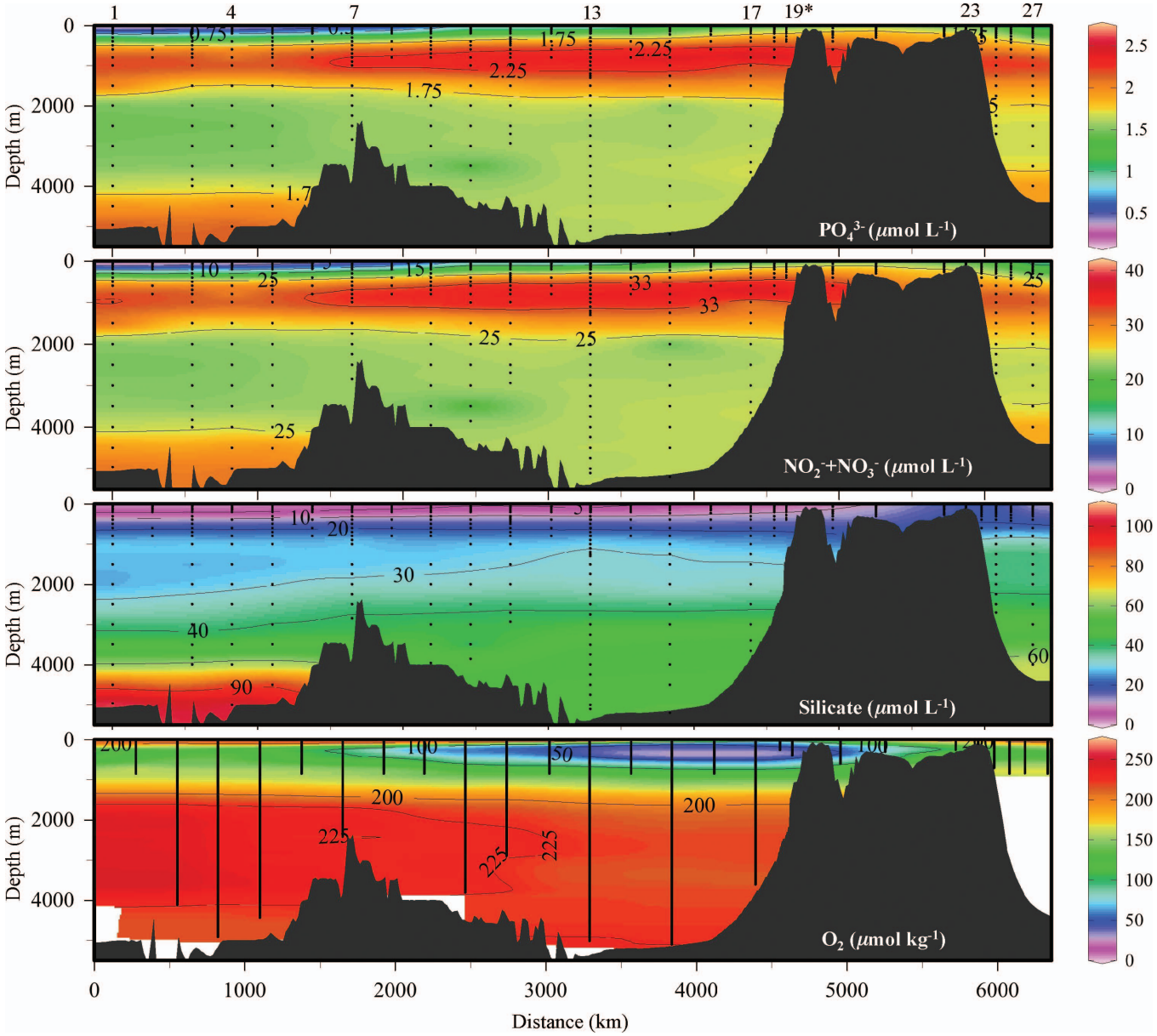

Fig. 2. Full-depth ocean sections of macronutrients, and oxygen for the CoFeMUG expedition. There is an OMZ in the eastern end of the basin due to high productivity and subsequent organic matter decomposition and the limited water mass ventilation.

Sampling and analysis of N_2O—Nitrous oxide (N_2O) samples were collected from the trace metal rosette by twice overfilling glass 165-mL serum bottles (Wheaton) using Tygon tubing. They were poisoned with 100 μL of saturated $HgCl_2$ solution and then sealed with butyl stoppers (MicroLiter Analytics) and aluminum crimps. Poisoned samples were stored for at least 2 months before analysis; however, previous research has demonstrated the integrity of this storage method for up to 6 months (McIlvin and Casciotti 2011). Isotopic analyses of N_2O

←

Fig. 1. Cruise track with station locations and full-depth ocean sections of total dissolved cobalt, labile cobalt, total dissolved iron, and total dissolved manganese for the CoFeMUG expedition across the Southern Atlantic Ocean. A large plume of cobalt, with corresponding but smaller plumes of iron and manganese, originates at the Southwest African coast and extends to the center of the basin. Coastal sources are likely due to a combination of reductive dissolution and resuspension of particulate matter in the sediments along the shelf. A plume of iron and manganese also extends westward from the Mid-Atlantic Ridge, with no corresponding elevated concentrations for cobalt (M. A. Saito and A. E. Noble unpubl.). Note that the main transect (E–W), the meridional transect along the Namibian coast (N–S), and the southern zonal transect (W–E) are connected to form a continuous wraparound section for each analyte, by cruise track distance from Sta. 1, numbered sequentially. The asterisk marks the end of the main transect.

Table 1. SAFe (S1 and D2) and GEOTRACES (GS and GD) standard seawater cobalt analysis results for UV-digested samples. All values are in pmol L^{-1}. nd, no data available.

Sample	Dec 08	Aug 10	Oct 10	Current consensus
S1	7±1.4(n=5)	4±2.9(n=4)	nd	5.4±2.2
D2	49±5.8(n=5)	45±2.9(n=2)	nd	45.4±3.8
GS	31±1.7(n=4)	25±1.2(n=4)	31±2.9(n=7)	35±7
GD	70±5.3(n=4)	59±5.2(n=6)	70±5.2(n=9)	65±8

were made using a Finnigan Delta^{PLUS} XP isotope ratio mass spectrometer (McIlvin and Casciotti 2010).

Nutrient and oxygen analyses—Nutrient samples were filtered and frozen in acid-washed 60-mL high-density polyethylene bottles until analysis. The frozen samples were thawed in a warm water bath and stored in the dark for 20–24 h prior to analyses. This protocol has been found to increase the recovery efficiency of silicic acid in frozen samples, and has no observed adverse effects on the other nutrients. Immediately before analysis, aliquots of the samples were transferred to 15-mL polypropylene cups and an Alpkem autosampler. Technicon AutoAnalyzer II™ components were used to measure phosphate and ammonium; and Alpkem rapid flow analyzer (RFA) 300™ components were used for silicic acid, nitrate + nitrite, and nitrite. All five of the macronutrients were analyzed simultaneously. The nutrient methods were essentially those employed by the Oregon State University lab during the World Ocean Circulation Experiment and Southern Ocean Joint Global Ocean Flux Study (JGOFS) cruises. The phosphate method was a modification of the molybdenum blue procedure of Bernhardt and Wilhelms (1967), in which phosphate was determined as reduced phosphomolybdic acid employing hydrazine as the reductant. The nitrate + nitrite analysis used the basic method of Armstrong et al. (1967). Sulfanilamide and *N*-(1-napthyl) ethylenediamine dihydrochloride react with nitrite to form a colored diazo compound. For the nitrate + nitrite analysis, nitrate is first reduced to nitrite using an open tubular cadmium reductor and imidazole buffer as described by Patton (1983). Nitrite analysis was performed on a separate channel, omitting the cadmium reductor and the buffer. The determination of silicic acid was based on that of Armstrong et al. (1967) as adapted by Atlas et al. (1971). Addition of an acidic molybdate reagent forms silicomolybdic acid, which is then reduced by stannous chloride. An indophenol blue ammonium method was modified from Alpkem RFA methodology, which references Methods for Chemical Analysis of Water and Wastes, March 1984, EPA-600/4-79-020, "Nitrogen Ammonia," Method 350.1 (Colorimetric, Automated Phenate). A detailed description of the continuous segmented flow procedures used can be found in Gordon et al. (1994).

Oxygen sensor data were calibrated by five Winkler titrations performed at Sta. 1, 2, 13, 22, and 24. Oxygen data were obtained from the conductivity, temperature, depth rosette Sea-Bird sensor (SBE-43) at every station (0–800 m) and at every deep station (full depth) from the trace metal rosette Sea-Bird SEACAT SBE-19 sensor. Titration water samples were taken immediately after rosette recovery by overfilling volume-calibrated flasks by one flask volume and then sealing with ground-glass stoppers. Standard Winkler reactions with iodate standards were performed and used to calibrate the Sea-Bird sensor and SEACAT sensor data. In cases where data were available from both sensors, the SBE-43 sensor data were used rather than the SEACAT sensor data due to its closer relationship to the calibration titrations (r^2 = 0.9995 and 0.995 for Sta. 1 and 13, respectively).

Particle trap collection and analysis—Sinking particulate matter was collected using a surface-tethered, drogued-at-depth system and acid-cleaned polycarbonate particle interceptor tubes, similar to that used during JGOFS and at Hawaii Ocean Time Series and Bermuda Atlantic Time Series (Steinberg et al. 2001). Collection tubes were held in polyvinyl chloride frames at depths of 60, 150, and 500 m at Sta. 13, and only the shallower two depths at Sta. 19. Six to eight tubes were deployed at each depth, and held 250 mL of a double-strength seawater brine (made by freezing filtered uncontaminated local seawater) at the bottom of each tube below a layer of filtered seawater that was buffered with borate to pH 8.2 and that doubled the alkalinity. No additional preservative was used, and we have found that for short-duration deployments, brine without preservative gives comparable fluxes of carbon, nitrogen, and thorium as did brines preserved with formaldehyde (Lamborg et al. 2008). The system was deployed for 3 d at Sta. 13 and 4 d at Sta. 19. Two capped tubes, loaded with filtered water and brine, were onboard the array and used as a process blanks, and subjected to all the same processing protocols as the samples. After recovery, the tubes were allowed to stand for $>$ 1 h and brine and particle mixture screened (350 μm) to remove zooplankton swimmers. The remaining particles were collected onto acid-cleaned and pre-weighed 25-mm-diameter, 1-μm-pore-size polycarbonate Nuclepore filters. Following the filtering, the membranes were rinsed with a small amount of pH 8.2, borate-buffered Milli-Q water. Prior to analysis, samples were desiccated and weighed cleanly in a laminar flow bench. Minor and trace elements were determined by ICP-MS as described in Lamborg et al. (2008).

Suspended particle collection and analysis—Size-fractionated particles were collected via in situ pumps (McLane Research Laboratories, Inc.) on McLane-style filter holders. The $>$ 51-μm size fraction was collected on acid-cleaned polyester prefilters (Sefar), followed in-line by collection of the 1–51-μm size fraction on combusted, acid-cleaned quartz microfiber filters (Whatman QMA). Process blank filters were a complete filter set that was loaded in a plastic housing, attached to a pump, and deployed. These "dipped blank" filters were exposed to seawater but did not have water actively pumped through them, and were otherwise processed identically. QMA subsamples were digested in Teflon bombs (Savillex) in 50% v v^{-1} nitric acid (Seastar Baseline) for 4 h at 135°C, centrifuged to remove filter slurry, and diluted to 5% v v^{-1} HNO_3 for

analysis by ICP-MS (Thermo Element2). Indium was used as an internal drift monitor, and concentrations were determined using multielement external standard curves. The recovery of manganese, cobalt, and iron from the MESS-3 sediment standard using this digestion procedure was 97%, 94%, and 84%, respectively, of certified values. All reported concentrations have had the process blanks removed. Sample handing and analyses were all conducted in class-100 clean environments following trace metal procedures.

Data analysis and repository—Linear relationships between cobalt and phosphate, oxygen, N_2O, and $\delta^{15}N$ were determined by applying a two-way linear regression least squares fit in MATLAB (MathWorks Inc.) using the script lsqfitma.m. The cobalt plume size calculations were determined by creating a grid of the South Atlantic basin, where each sampling point represented the corner of an enclosed area (either trapezoidal or triangular in shape). The area of each box was determined by depth and distance between data points, and the total cobalt in each box was determined by calculating trapezoid areas to interpolate between sampling points across the basin. The plume was defined by the 100 μmol kg^{-1} O_2 contour where the elevated cobalt was found. The cobalt within the plume was divided by the sum of the cobalt within the upper 1000 m to estimate relative inventories. The trace metal data presented in this paper (429 total dissolved iron values, 429 total dissolved manganese values, 346 total cobalt values, and 290 labile cobalt values, with fewer than 7 outliers for each species analyzed) have been deposited into the Biological and Chemical Oceanography Data Management Office database under the CoFeMUG program (http://bcodmo.org/). Ocean sections were created in Ocean Data View with the exception of these few outliers (Schlitzer 2011).

Results

The CoFeMUG expedition consisted of three transects: The main zonal transect (Sta. 1–19; main transect hereafter), a short meridional transect along the coast within the Benguela Upwelling (Sta. 19–23), and a short transect south of the main transect extending from the shelf back into the gyre (Sta. 23–27; southern transect hereafter). The cruise proceeded from west to east across the basin, from regions of low productivity in the oligotrophic subtropical gyre to higher productivity in the Angola Gyre and finally to the highest productivity regions associated with coastal upwelling of macronutrients (Figs. 1, 2). The high-productivity coastal regions were further distinguished by water masses of the Angola Dome (the southern edge of which is observed in Sta. 17 and 18), the Benguela Upwelling region that covers much of the Namibian and South African Atlantic coast (Weeks and Shillington 1994), and the dynamic Angola-Benguela Frontal Zone (ABFZ) that lies between them (roughly between 14.5°S to 18.5°S for the northern and southern extents varying by season and climatology; Kostianoy and Lutjeharms 1999; Lass and Mohrholz 2008).

Dissolved metal distributions and regional oceanography—The western and central region of the main transect sampled the oligotrophic subtropical gyre and was characterized by surface drawdown of total cobalt to 6 pmol L^{-1}, labile cobalt to below detection, and iron to 0.05 nmol L^{-1}, while surface manganese concentrations remained consistently elevated across the entire main transect with values ranging from 1.93 to 4.04 nmol L^{-1} (Figs. 1, 3). Along the coast of Namibia, elevated concentrations of all three metals were found that extended far into the South Atlantic basin along the main transect. For example, in the upper 60 m of Sta. 18 and 19, concentrations reached as high as 200 pmol L^{-1} Co, 4.04 nmol L^{-1} Mn, and 3.03 nmol L^{-1} Fe with a second, spatially pronounced, westward propagating feature for all three metals observed around 400 m (163 pmol L^{-1} Co, 3.1 nmol L^{-1} Fe, 1.1 nmol L^{-1} Mn; Figs. 1, 3, 4). Of the three metals, the subsurface cobalt extended farthest into the basin, for a distance of approximately 2500 km from the Namibian coast. This cobalt plume comprised 37% of the upper 1000 m of the zonal section area, but disproportionately contributed 53% of the total cobalt therein (Fig. 4; *see* Methods for calculations). The potential contributions to this cobalt plume are discussed in later sections.

Within the Angola Gyre, the edge of the Angola Dome is identified by a high temperature signature at Sta. 17 and 18 between 0- and 50-m depth (Lass and Mohrholz 2008; Fig. 5g). Cobalt, iron, and manganese concentrations at 400 m were 2.2, 3.8, and 3.8 times higher in the Angola Gyre (Sta. 15–19), respectively, than at comparable depths in the center of the oligotrophic subtropical gyre (Sta. 3–5), and 2.6, 2.5, and 1.9 times higher than at comparable depths off the coast in the southern transect (Sta. 25–27). The elevated metals generally co-occurred with the oxygen depletion that occurs as a result of organic matter remineralization and poor ventilation in the shadow zone near the African coast (Figs. 2, 4, 5a; Lass and Mohrholz 2008; Mohrholz et al. 2008). South Atlantic Central Water (100–500 m) carries this low oxygen signature south and eventually westward upon convergence with Eastern South Atlantic Central Water (Mohrholz et al. 2008). Additional oxygen consumption is driven by the Benguela Upwelling to the south, which also injects nutrients into surface waters.

In contrast to the high abundances observed offshore in the main transect through the Angola Gyre (Fig. 4), the cobalt, iron, and manganese concentrations were lower in the offshore southern zonal transect (Fig. 1). Metal concentrations were high along the coast at Sta. 23, reaching 203 pmol L^{-1} Co, 7.9 nmol L^{-1} Fe, and 2.8 nmol L^{-1} Mn, and dissolved oxygen was low (as low as 11 μmol kg^{-1}), but this signal did not extend westward at this latitude. This likely reflects the differences in physical processes where the main transect encounters surface and subsurface westward advection resulting from the convergence of the southward-flowing Angola Current and the northward-flowing Benguela Coastal Current (at the ABFZ) and from the northwestward-flowing Benguela Ocean Current that is driven by the strong trade winds

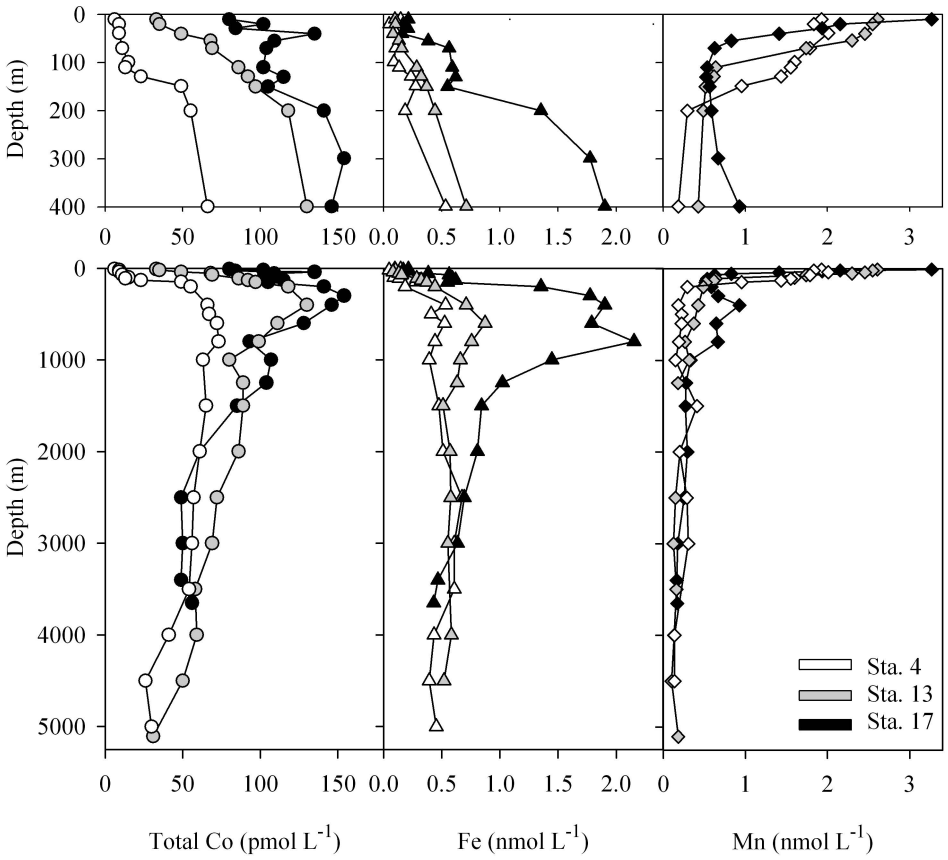

Fig. 3. Representative vertical profiles from the CoFeMUG data set, showing the subsurface maxima for cobalt, iron, and manganese with proximity to the coast.

(Peterson and Stramma 1991; Mohrholz et al. 2008). In contrast, the southern zonal transect crossed the northward-flowing Benguela Coastal Current where it likely still follows the coastline north, and water mass movement westward is more restricted (Peterson and Stramma 1991).

A discussion of the hydrothermal contributions of iron and manganese plumes found above the Mid-Atlantic Ridge (M. A. Saito unpubl.) will be presented elsewhere. Lastly, strong correlations between cobalt and phosphate are observed in surface waters, and a discussion of the ecological stoichiometry of cobalt in this region relative to the North Atlantic (A. E. Noble unpubl.) will also be presented elsewhere.

Particulate distributions—Particulate phosphorus, cobalt, iron, and manganese concentrations are presented for a coastal station (Sta. 19) and an open-ocean station (Sta. 13). For all elements, the particulate concentrations observed at the coastal station were higher than were observed at the open-ocean station.

At the coastal station, dissolved and particulate cobalt, iron, and manganese showed parallel trends with depth (Sta. 19, Fig. 6f–h), and in all cases but that of iron, the relative concentrations of the particulate material were orders of magnitude lower than that of the dissolved counterpart ($pP : dPO_4^{3-} \approx 1 : 780$, $pCo : dCo \approx 1 : 25$, $pMn : dMn \approx 1 : 6$ along the coast and $pP : dPO_4^{3-} \approx 1 : 4260$, $pCo : dCo \approx 1 : 180$, $pMn : dMn \approx 1 : 14$ within the gyre, p = particulate and d = dissolved; Fig. 6). Particulate iron concentrations increased at Sta. 19 to values that were 7 times higher than the dissolved counterpart (Fig. 6g). While particulate cobalt concentrations also increased at the bottom sampled depths (Fig. 6f), the dissolved counterpart was ~ 20 times higher than the particulate concentrations, and a similar trend was observed for manganese (dMn ~ 10 times pMn) (Fig. 6h).

At the open ocean station, particulate profiles exhibited surface maxima for cobalt and phosphorus but not for iron and manganese (Sta. 13, Fig. 6a–d). Instead, particulate iron and manganese showed steady increases in concentration from the surface to 600 m (Fig. 6c,d), and the particulate concentrations were respectively 140- and 6-fold less than the respective coastal particulate concentrations (P. Lam and D. Ohnemus unpubl.; Fig. 6c,d,g,h).

Particle fluxes—Sediment trap data are reported at 60-, 150-, and 500-m depth for an open-ocean station (Sta. 13), and at 60- and 150-m depth for a coastal station (Sta. 19). At the open-ocean station, the trap data showed a decrease in flux with depth between the 60-m and 150-m traps (Fig. 7b–e). The integrated input from remineralization was calculated by taking the difference between the fluxes and dividing it by the depth between the two traps. By this estimate, remineralized metal fluxes of 0.013 pmol Co

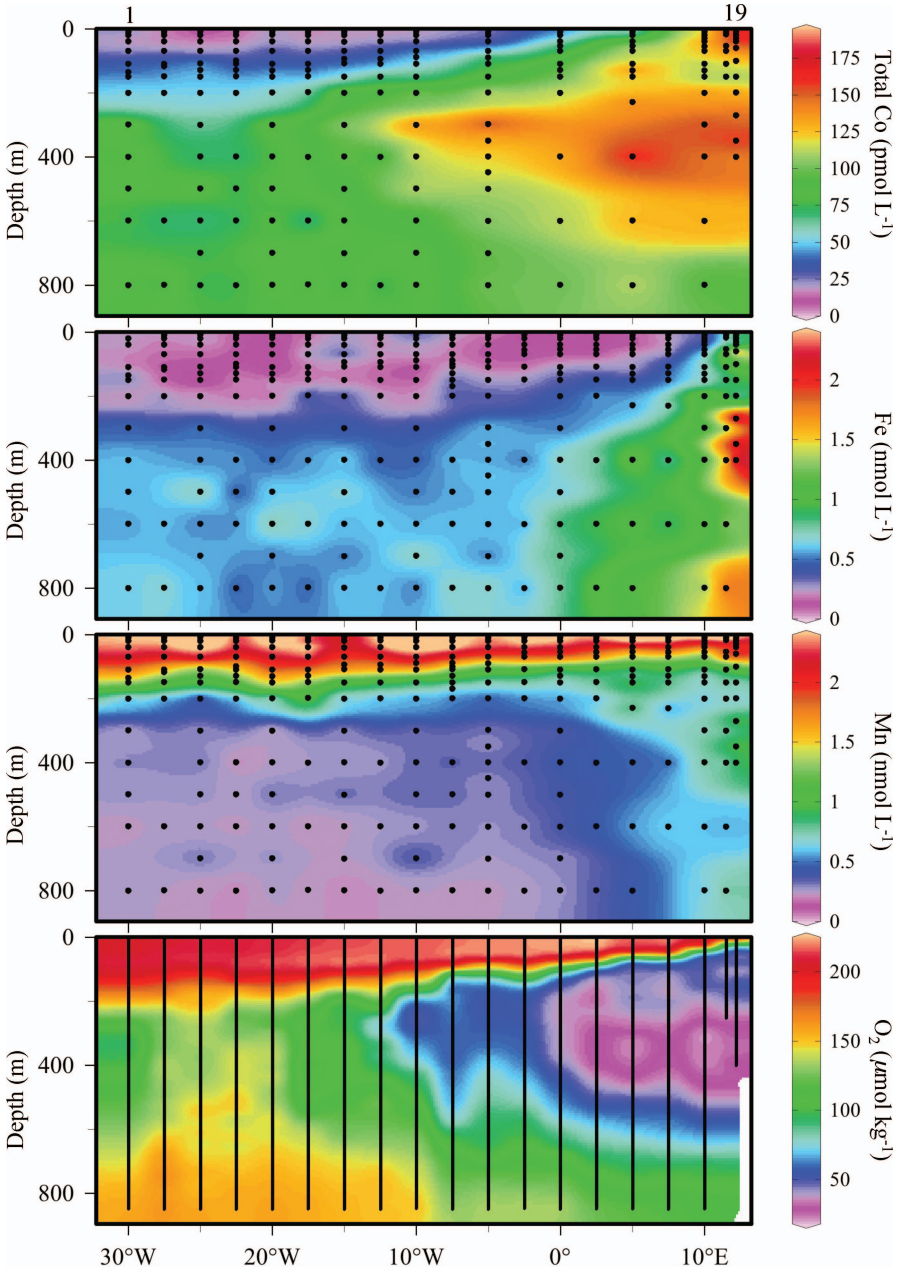

Fig. 4. Expanded upper water column sections for the northern transect. Metal concentrations decrease with distance from the coast, and the coincidence of the OMZ with iron, manganese, and particularly cobalt, is evident. For reference, the Mid-Atlantic Ridge is centered over 15°W.

L^{-1} d^{-1}, 8.5 pmol Fe L^{-1} d^{-1}, 0.11 pmol Mn L^{-1} d^{-1}, and 11.2 nmol P L^{-1} d^{-1} were delivered to the water column between these sediment trap depths.

At the coastal station, the 60-m flux was indistinguishable from the open-ocean flux within the error of the measurement. The sediment trap data did not detect remineralization for iron, manganese, and phosphorus (Sta. 19, Fig. 7b,d,e); however, the total mass flux at 150 m was larger than that at 60 m, with no noticeable change in the iron, manganese, and phosphorus fluxes (Fig. 7a,b,d,e), which may be due to particulate cycling processes other than remineralization.

Discussion

The overarching scientific objective of this research cruise was to examine the distributions of cobalt, iron, and manganese in the OMZ of the South Atlantic and Benguela Upwelling Region, motivated by previous observations of elevated cobalt in the OMZs of both the Costa Rica Dome and the Peru Upwelling Region (Saito et al. 2004, 2005). The metal distributions within three broad geographic distinctions are presented in this paper: the low surface concentrations in the oligotrophic gyre, the large plumes observed within the subsurface OMZ of the South

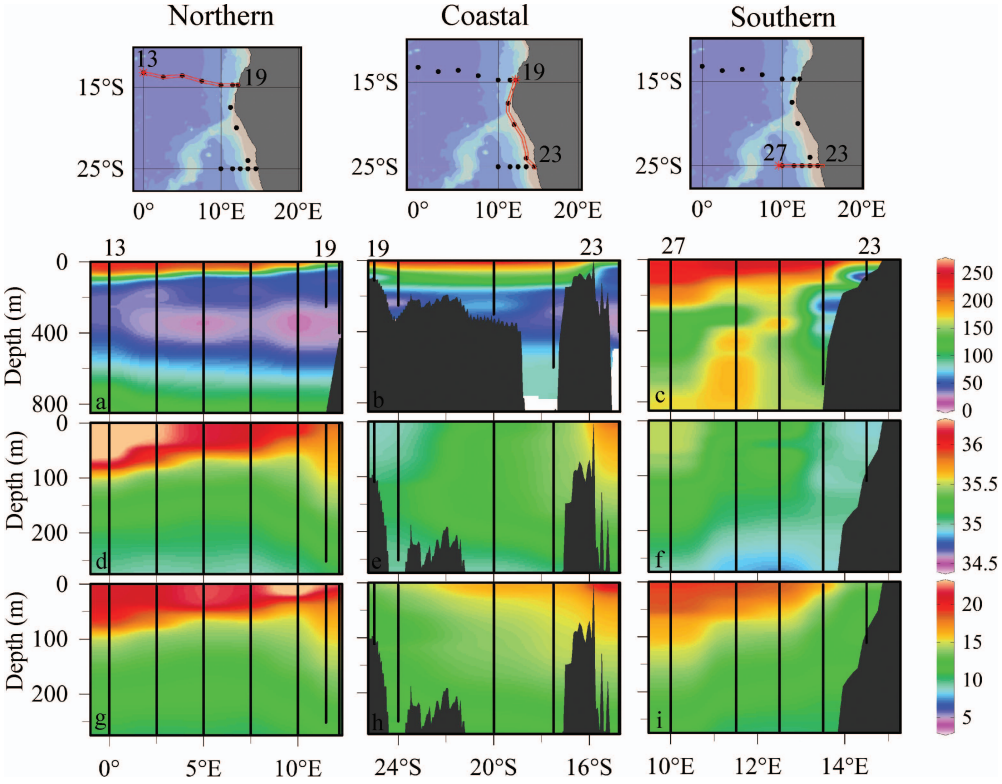

Fig. 5. Hydrographic distributions in the northern, coastal, and southern transects near the Southwest African coast for the (a–c) dissolved oxygen (μmol kg^{-1}) in the upper 800 m, (d–f) salinity in the upper 300 m, and (g–i) potential temperature (°C). Oxygen concentrations are much higher in the southern transect than in the northern and coastal transects, and low-oxygen waters along the coast do not appear to be advected westward in the south as they are in the north.

Atlantic, and the localized, elevated concentrations along the coast. The salient, large basin-scale features apparent in the ocean section are presented first, followed by the coastal observations and discussion of potential supply mechanisms.

Upper Ocean distributions of dissolved cobalt, iron, and manganese—The oligotrophic waters of the western and central regions of the main transect were characterized by surface drawdown of total cobalt, labile cobalt, and iron due to biological utilization (Figs. 1, 3). These low surface cobalt and iron concentrations (6 pmol L^{-1} and below detection for total and labile cobalt, respectively, 0.05 nmol L^{-1} iron) were within a range that can be limiting to some phytoplankton growth (Sunda and Huntsman 1995), although a few stations may reflect some aeolian deposition that could relieve micronutrient stress (Sta. 9, 10 m; 0.34 nmol L^{-1} Fe, 6 pmol L^{-1} labile Co). These low surface concentrations are consistent with modeling studies by Mahowald et al. (2005) that predict low dust input to the South Atlantic (Fig. 8a), relative to large inputs like the Sahara Desert to the north (Vink and Measures 2001).

In contrast to cobalt and iron, manganese remained consistently elevated in surface waters across the entire main transect, with values ranging from 1.93 to 4.04 nmol L^{-1}. While this surface maximum is typical of manganese profiles from tropical and subtropical regions, its uniformity across the region is perhaps surprising. Aeolian deposition is often invoked as a primary source of manganese to the surface ocean (Statham et al. 1998). Given the low dust deposition predicted for this region (Fig. 8a), these observations suggest that there is likely an additional mechanism working to maintain the uniform surface maxima, such as redox cycling processes that act to retain dissolved manganese at the surface. Manganese-oxidizing bacteria are photoinhibited in the mixed layer, but below that, they are known to oxidize manganese, creating small neutrally buoyant manganese oxide particles that may be re-entrained into the mixed layer and photoreduced (Sunda and Huntsman 1988; Tebo et al. 2004). The combination of aeolian input from above and entrainment and recycling of manganese oxides from below could act to create and maintain the elevated dissolved manganese surface-water inventory we observe across the gyre, similar to redox processes that can concentrate dissolved and particulate metals at distinct strata in sedimentary environments.

Elevated concentrations of cobalt, iron, and manganese were found along the coast of Namibia and extended into the South Atlantic basin in the main transect (Fig. 4). Subsurface cobalt concentration at around ~ 400 m extended farthest into the basin, for a distance of ~ 2500 km from the Namibian coast. As described in the Results section above, this cobalt plume spatially made up 37% of the upper 1000 m of the zonal section, but

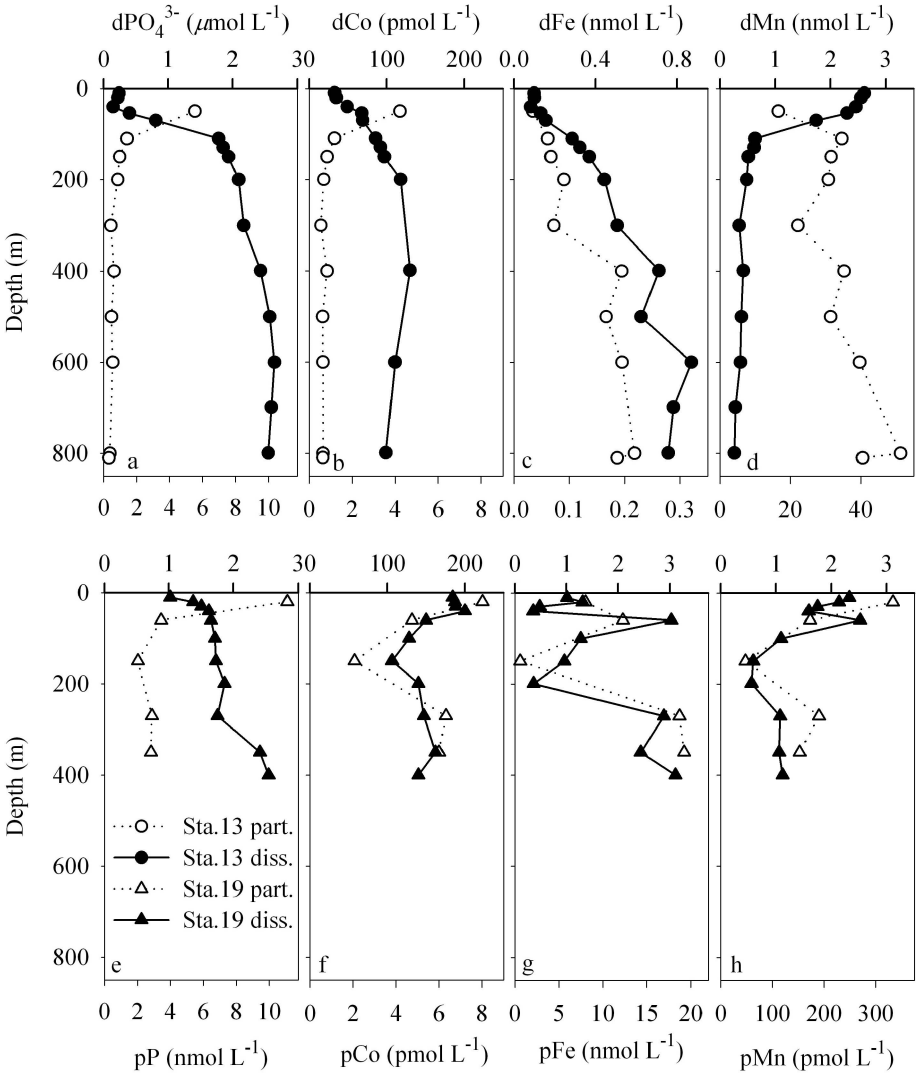

	dissolved	particulate	spatial observations
Co	low scavenging	coastal > open ocean	$dCo_{coast} >> pCo_{coast}$ $dCo_{basin} >> pCo_{basin}$
Fe	high scavenging	coastal >> open ocean	$dFe_{coast} < pFe_{coast}$ $dFe_{basin} \approx pFe_{basin}$
Mn	moderate scavenging	coastal > open ocean	$dMn_{coast} > pMn_{coast}$ $dMn_{basin} > pMn_{basin}$

Fig. 6. Trace metal particulate (open symbols, bottom axes) and dissolved (filled symbols, top axes) profiles for the upper 800 m from (a–d) Sta. 13 and (e–h) Sta. 19. Dissolved concentrations of phosphorus, cobalt, and manganese far surpass that of their respective particulate concentrations; however, the particulate concentrations of iron are approximately 5 times higher than that of the dissolved phase. A brief schematic is presented beneath the profiles to summarize the observations for each metal and facilitate comparison.

disproportionately contributed more than half of the total cobalt therein (Fig. 4). There are two potential causes of these plumes. First, these metals could be released from coastal sedimentary sources and advected westward. Second, the plumes could be formed by the remineralization of exported particulate organic matter from the euphotic zone. Both of these mechanisms are consistent with regional circulation and high productivity, and hence a combination of these two processes likely contributes to the plumes, as discussed in later sections.

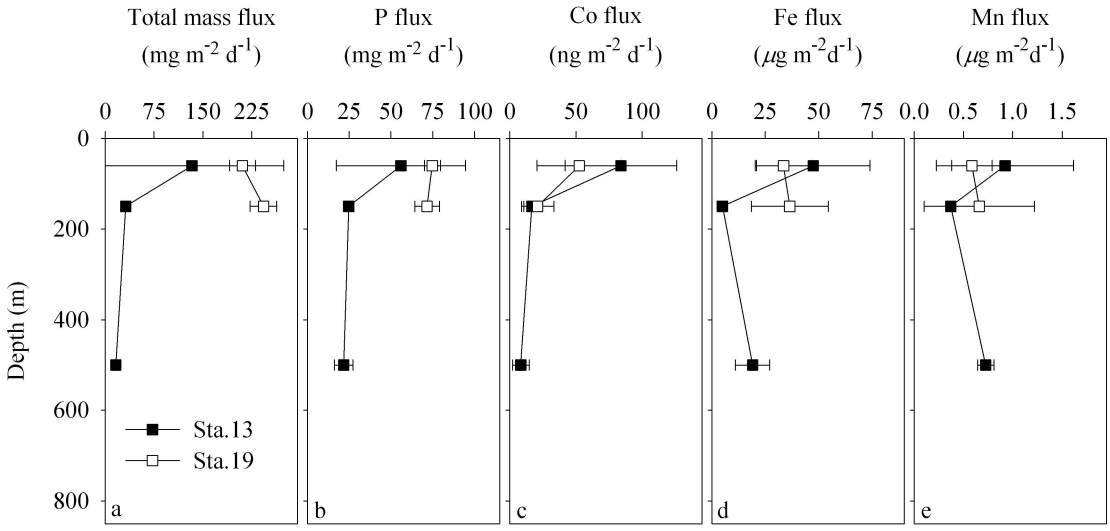

Fig. 7. Sediment traps were deployed at Sta. 13 (black squares, open ocean) and 19 (white squares, coastal) for 3 and 4 d, respectively. As expected, the productive coast shows a higher total mass flux and total P flux (a proxy for biologically generated particulate matter) than the oligotrophic gyre. In addition, the Sta. 19 total mass flux at 150 m is greater than the flux at 70 m, suggesting that some horizontal particle movement may be occurring. Error bars were calculated as the standard deviation of triplicate measurements.

In order to compare cobalt, iron, and manganese biogeochemical cycles in the South Atlantic Basin, the sources and sinks acting on this system are described based on our current understanding. This includes estimates of relative differences in removal timescales for these metals, a discussion of the potential role of sediments and dust as sources, and consideration of lateral and vertical mechanisms for delivery of metals to the basin.

Cobalt, iron, and manganese plumes across the South Atlantic basin—One of the striking observations in this data set is the differing extent to which cobalt, iron, and manganese penetrate into the subsurface OMZ of the South Atlantic Gyre (Figs. 1, 4). While cobalt extends farthest, more than halfway across the northern zonal transect, and shows an inverse linear correlation with oxygen (Fig. 9), iron and manganese show exponential removal relative to both distance from the coast and oxygen. Their differing reaches into the basin could be explained by differences in each metal's scavenging rates upon the horizontally advected and vertical remineralized flux, and/or by differences in supply from remineralized vertical flux, for example by changes in the Co : Mn : Fe stoichiometry of exported material. For horizontal advection, mixing and scavenging control the dissipation of the coastal signal as water flows westward with time, and since mixing should affect these metals identically, scavenging likely controls the observed differences in the subsurface distributions. Iron and manganese show exponential removal when compared to distance from coastal source waters and oxygen (Fig. 10e–h). Concentrations along the 27.0–27.1 density layer (400-m depth) approach 0.55 nmol L^{-1} Fe (0.2 nmol L^{-1} for Mn) at the western end of the basin where oxygen concentrations also plateau, which may represent some fraction of the dissolved pool that is protected from biotic or abiotic scavenging by binding to strong organic ligands over time (Johnson et al. 1997). As a result, the aggregate scavenging behavior (k_{scav}) can be described by fitting a curve to the data using a simple parameterization representing biotic or abiotic processes:

$$[M]_x = [M]_{x-1} - \left([M]_{x-1} - [M]_L\right) k_{scav} d_x \quad (1)$$

In this equation, $[M]_x$ is the metal concentration in mol L^{-1} at a distance x, $[M]_{x-1}$ is the concentration of metal at an "upstream" sample location at the same depth, and $[M]_L$ is the concentration of metal that is presumed to be protected from scavenging by binding to organic ligands. The longitudinal distance between one data point ($[M]_{x-1}$) and the next ($[M]_x$) is denoted by d_x. This simple equation assumes that metals are being scavenged along a westward path, and does not account for additional vertical input. Empirically estimating $[M]_L$ to be the asymptotic concentration observed in the western end of the basin, and defining $[M]_{x=0}$ to be the observed concentration in the eastern end of the basin, the relative removal rates for each metal were estimated. A nonlinear fit to the iron concentrations at 400 m suggests a 0.0025 km^{-1} scavenging rate. If oxygen concentrations reached extreme lows, they may influence the pseudo first-order rate constant by reducing the oxidation rate (assuming scavenging is redox-mediated). It appears, however, that the oxygen concentration range we observe here is likely still too high to decrease either iron or manganese scavenging significantly. Estimating manganese scavenging by the same approach, and using 0.20 nmol L^{-1} for $[M]_L$, we calculate a scavenging rate of 0.001 km^{-1}, which is 2.5 times slower than the rate observed for iron.

In comparison to iron and manganese, cobalt appears to be insensitive to scavenging within the OMZ, indicated by an inverse correlation with oxygen (r^2 = 0.73), as observed

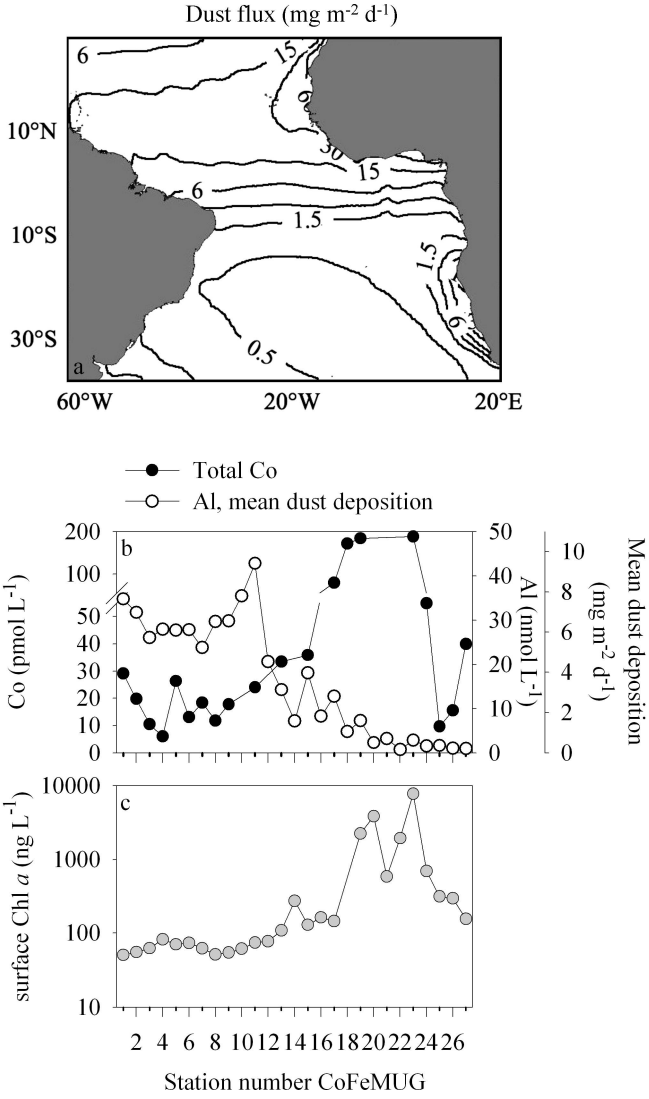

Fig. 8. (a) Estimates of dust input to the South Atlantic region, generated using data and a model generously provided by N. Mahowald (Mahowald et al. 2005). Inputs of dust are estimated to be much higher in the North Atlantic than the South Atlantic. (b) Surface transect of total dissolved cobalt and dissolved aluminum showing an opposite relationship, suggesting that the high dissolved cobalt near the coast is not derived from dust. (c) Measured surface Chl *a* concentrations.

previously in the Angola Dome (Pohl et al. 2011), and also by a correlation with N_2O ($r^2 = 0.80$) (Fig. 9a,b). If higher oxygen concentrations were increasing cobalt oxidation kinetics and scavenging, one would expect to see a relationship similar to that observed for iron and manganese. Because this is not observed, it suggests that cobalt scavenging rates were slower than physical mixing processes or that cobalt concentrations are at steady state, where scavenging rates were slow enough to be equally matched by lateral and vertical input (Fig. 10c,d). The cause of the $Co : N_2O$ relationship is unknown, and while the source mechanisms of these species may not be directly connected, their general coastal source locations likely are. The advection and persistence of these two chemical species with similarly slow removal timescales could lead to the observed correlation. There could also be specific mechanistic, enzymatic, or chemical explanations for the correlation. For example, NO and N_2O are often produced through the same processes (Yoshida 1988) and NO levels can be elevated in low-oxygen waters (Ward and Zafiriou 1988). Cobalt-containing cobalamin and cobinamide molecules are known to have high affinities for NO (Sharma et al. 2003), and it may be possible that elevated NO concentrations stabilize labile cobalt and protect it from scavenging.

Using Eq.1, the relative removal of cobalt was estimated to be 0.0003 km^{-1} at 400 m. This low value likely primarily reflects mixing processes since there is no mixing term in Eq. 1 and exponential removal was not observed. $[M]_L$ was calculated by taking the average difference between the total and labile cobalt concentrations at 400, 600, and 800 m in the western end of the basin (Sta. 1–9), and was determined to be quite uniform with concentrations of 68 ± 15.9 pmol L^{-1} ($n = 8$) at 400 m, 60 ± 11.0 pmol L^{-1} ($n = 7$) at 600 m, and 60 ± 8.9 pmol L^{-1} ($n = 8$) at 800 m. The decrease in standard deviation with depth may be reflective of more uniform concentrations of cobalt at depth and less biological and chemical variability.

The observation that cobalt persists much farther westward than manganese in the OMZ is intriguing since previous process studies have demonstrated that these metals are linked by a common scavenging mechanism: the oxidation by manganese-oxidizing bacteria (Tebo et al. 1984; Moffett and Ho 1996). The cobalt and manganese concentrations in the coastal end-member are enriched (0.200 nmol L^{-1} and 2.0 nmol L^{-1}, respectively) relative to their oceanic deep-water concentrations (0.045 nmol L^{-1} and 0.20 nmol L^{-1}, respectively), yet unlike cobalt, these enhanced coastal manganese abundances do not result in a significant plume. There are several possible explanations for this difference. First, cobalt is present in much lower concentrations than manganese (0.006–0.200 nmol L^{-1} for Co vs. 0.10–4.03 nmol L^{-1} for Mn); thus, the elevated cobalt concentrations in the plume may be below concentrations at which a quantitatively significant coupling between manganese and cobalt scavenging might be observed. Second, manganese scavenging may be more apparent due to its preferential oxidation relative to cobalt (Moffett and Ho 1996). This notion is supported by the differences in the dissolved to particulate trace metal ratios for cobalt (dCo : pCo) and manganese (dMn : pMn) at Sta. 13 (Fig. 6), where dCo : pCo was 5–20 times higher than dMn : pMn below ~ 150 m. Third, oxygen concentrations may be low enough that microbially mediated oxidation of cobalt is kinetically unfavorable; we are unaware of studies examining the relative rates of oxidation of cobalt and manganese in low-oxygen environments. Fourth, the degree of cobalt and manganese complexation likely influences the relative scavenging and oxidation processes. Co(III), Co(II), and Mn(III) have been shown to form strong complexes with natural organic molecules and siderophores, respectively (Saito et al. 2005; Parker et al. 2007). The cobalt in the plume generally had > 75% of the total cobalt present in strongly complexed form (Figs. 1, 4), leaving less than a quarter of the labile cobalt available for

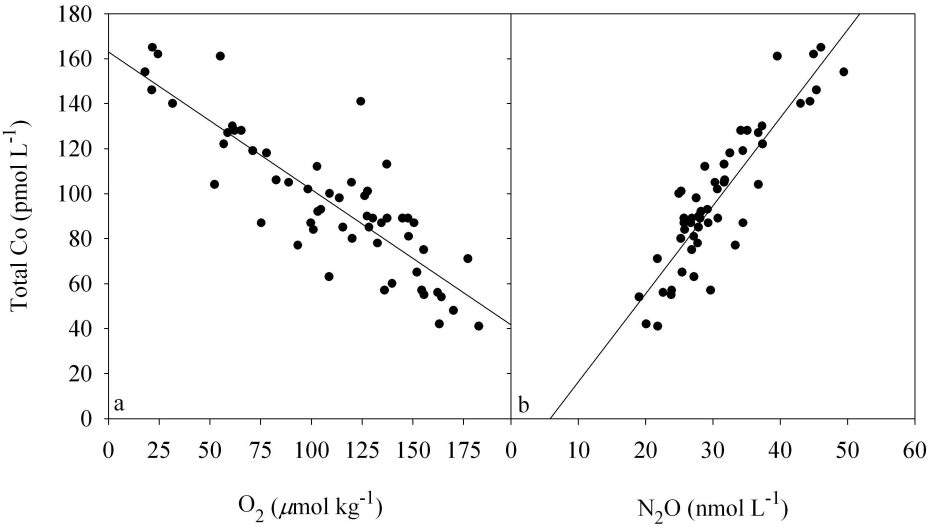

Fig. 9. Relationships between (a) oxygen and total dissolved cobalt and (b) N_2O and total dissolved cobalt for Sta. 5–27 between 300- and 800-m depth. The 300–800-m analyses showed a linear correlation between O_2 and Co ($r^2 = 0.73$). N_2O also shows a linear correlation with cobalt ($r^2 = 0.80$), suggesting that the two chemical species have similar coastal source locations.

co-oxidation, assuming complexed cobalt is not bioavailable to manganese-oxidizing bacteria. It is likely that the observed phenomenon is the result of a contribution from all four factors. There may be protection from scavenging by complexation for manganese as well, though little is known about the susceptibility of ligand-bound Mn(III) to bacterial manganese oxidation (Parker et al. 2007).

Implications for hybrid-type metals with ocean deoxygenation—A recent study by Stramma et al. (2008) found that the distribution of OMZs globally has increased significantly during the past 50 yr. Based on our observations within the South Atlantic OMZ, it seems possible that a coincident increase in ocean inventories of certain trace metals may occur with deoxygenation, particularly for the hybrid-type elements that have small oceanic inventories due to the confluence of nutrient uptake and intermediate-depth scavenging processes. The OMZ in the South Atlantic is relatively weak compared to the OMZs of the Pacific and Arabian Sea, where higher concentrations of dissolved iron and manganese have been observed (10 nmol L^{-1} Mn and 5 nmol L^{-1} Fe, Pacific, Martin et al. 1989; 2 nmol L^{-1} Fe, Arabian Sea, Moffett et al. 2007), consistent with this notion of a connection between low oxygen and hybrid-type metal flux. It is difficult to extrapolate the influence of intensified oxygen depletion on metal concentrations in the South Atlantic because of the complexities and uncertainties associated with estimating changes in the coastal sedimentary flux due to an expansion of regional low bottom-water oxygen (*see* Sedimentary metal source section). As a first approximation, we can use the linear relationship observed between cobalt and oxygen (Fig. 9), and a rate of oxygen depletion in the South Atlantic OMZ region of -0.17 μmol O_2 kg^{-1} yr^{-1} over the past 50 yr observed by Stramma et al. (2008). Using this deoxygenation rate, the cobalt inventory in the upper 1000 m of the South Atlantic Basin could increase $\sim$ 10% by the year 2100. An important potential effect of increased oceanic cobalt, iron, and manganese inventories is a stimulation of marine primary productivity and nitrogen fixation and/or changes in marine ecology driven by species with distinct trace element preferences. In particular, the nitrogen limiting conditions of the South Atlantic could be alleviated by increases in nitrogen fixation activity with an enhanced OMZ iron supply (Saito et al. 2011). If primary productivity and export were to increase, the resultant intensified remineralization would consume more O_2, creating a positive feedback mechanism for further expansion of OMZs. While the extent of this potential feedback mechanism may be limited by the phosphate inventory as the limiting factor for microbial nitrogen fixation, there is evidence for increased phosphate fluxes to the water column from sediments experiencing sustained bottom-water hypoxia due to dissolution of phosphate-bearing iron oxyhydroxide minerals (Reed et al. 2011). The South Atlantic also has a higher photic zone phosphate inventory than the North Atlantic (Fig. 2; Wu et al. 2000), however, suggesting that an increased coastal iron flux could contribute to this feedback mechanism prior to the onset of phosphate limitation. Future studies should investigate where the oxygen thresholds are with respect to reductions in metal scavenging rates, as well as the influence of expanded OMZs on coastal and sedimentary metal fluxes.

A sedimentary metal source—Cobalt, iron, and manganese concentrations increased with proximity to the Angolan and Namibian coasts, particularly between 200- and 1000-m depth. The source of these elevated metals is likely derived from the coastal sediments rather than aeolian deposition or riverine discharge. Coastal sediments can be a source of metals via dissolved fluxes from anoxic sediments and (or) particulate fluxes through resuspension of sedimentary material and subsequent desorption or dissolution in the water column. This source could reach

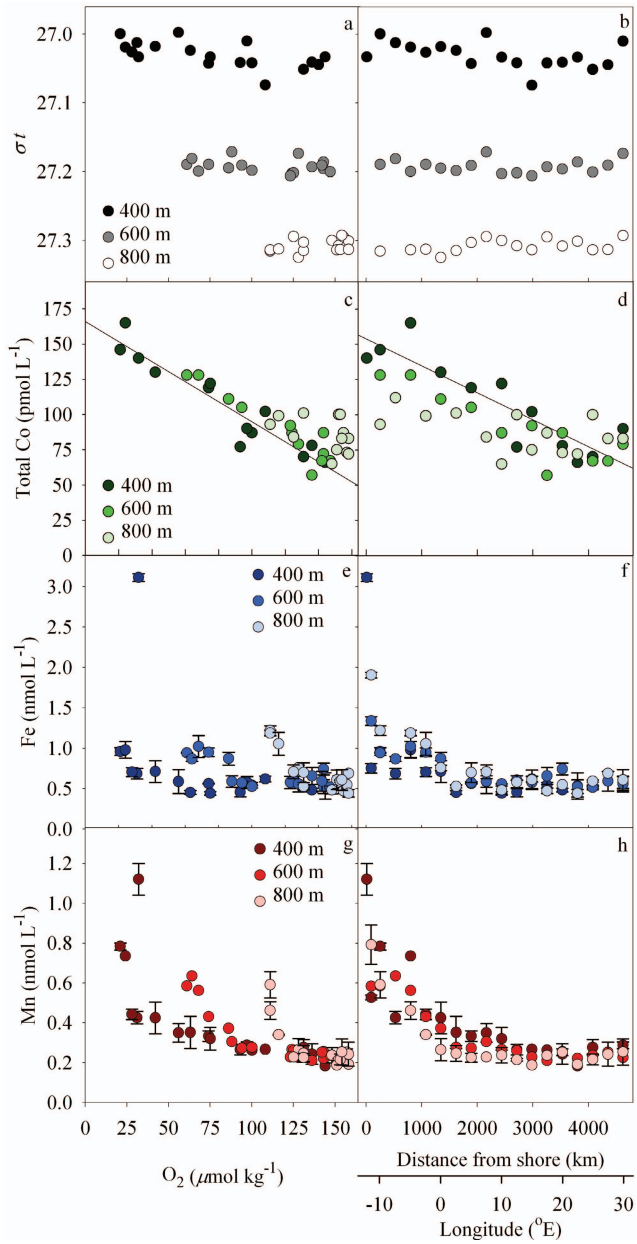

Fig. 10. Distributions of dissolved cobalt, iron, and manganese along isopycnal surfaces that correspond to 400-, 600-, and 800-m depths from the main transect. Potential density with respect to (a) oxygen and (b) distance are plotted at the three depths. Scavenging rates are estimated using Sta. 19 as the starting point and data to the west increasing in distance. Linear correlations between (c) total dissolved cobalt and oxygen, and (d) cobalt and distance are indicative of advection for both chemical species. The relationships between (e) iron and oxygen, (f) iron and distance, (g) manganese and oxygen, and (h) manganese and distance are all nonlinear. (f, h) When plotted as a function of distance, the data points fall along the same curve. Error bars here represent a standard deviation of two analyses, where in most cases, the first analysis was conducted in batches by profile over a number of discrete ICP-MS runs (10 d of analyses total), while the second analysis verified precision by analysis of all samples along each isopycnal on a single ICP-MS run. This approach verified that the day-to-day variability on the ICP-MS was not systematically affecting the isopycnal analysis.

the basin through both lateral (advection of coastal waters westward at depth) and vertical (dissolution and desorption in the euphotic zone and subsequent remineralization of sinking biogenic material) vectors. The relative importance of the processes that create these plumes likely varies for each metal, and the magnitude of dissolved and particulate fluxes from sediments can be influenced by advection, bottom-water oxygen concentration, and continental shelf width (Chase et al. 2005; Bruland et al. 2005; Lohan and Bruland 2008). Below, we discuss the potential sedimentary source mechanisms for each metal based on oxygen concentrations, dissolved and particulate trace metal abundances, and comparative transects over a narrow (northern) and broad (southern) shelf area in the Angola and Benguela regions.

Anoxic bottom-water conditions can generate metal fluxes from sediments by the reductive dissolution of metal-oxides and diffusion out of those sediments (Heggie and Lewis 1984; Johnson et al. 1988; Lohan and Bruland 2008). Critical to this process is the prevention of reoxidation by oxygen depletion at the sediment–water interface. The Namibian coastal shelf waters experience seasonal anoxia during the austral summer, coincident with detection of H_2S in bottom water due to sulfate reduction and occasional episodes of detectable methane (Bruchert et al. 2003; Emeis et al. 2004; Mohrholz et al. 2008). Conditions can even become reducing enough to allow for water column microbial sulfide oxidation, and a loss of nitrate due to denitrification and annamox (Lavik et al. 2009). Based on comparison of thermodynamic energy yields of redox couples, the presence of H_2S in the water column implies that more energetically favorable terminal electron acceptors, including manganese, iron, and cobalt oxide minerals, would have already been reduced and their soluble products released into pore waters. While precipitation of these reduced metals as metal sulfides might occur, aqueous sulfide complexes can form, and reduced metal maxima are often observed at the H_2S–O_2 interface, as has previously been observed in the anoxic Baltic Sea (Dyrssen and Kremling 1990). While reduced iron is sensitive to oxidative re-precipitation (Elrod et al. 2004), reduced manganese is less sensitive and reduced cobalt has been observed to diffuse the farthest of the three toward or past the sediment–water interface before oxidative re-precipitation (Klinkhammer 1980; Heggie and Lewis 1984). This reductive flux mechanism is likely occurring along the African shelf, and the highly reducing sediments here are likely instrumental in generating the cobalt plume observed in the zonal section (Figs. 1, 2, 4), as we have previously invoked to explain the high abundances in the north and south Eastern Subtropical Pacific (Saito et al. 2004, 2005). While the OMZ of the South Atlantic is generally considered to be much weaker than that of the Tropical Pacific, the observation of a plume here suggests that localized coastal anoxia may be more important than eventual OMZ oxygen levels in generating metal fluxes.

In recent years, the importance of advected particulate iron as a source to the oceanic iron inventory has been demonstrated (Lam et al. 2006; Lohan and Bruland 2008; Moore and Braucher 2008). The influence of advected

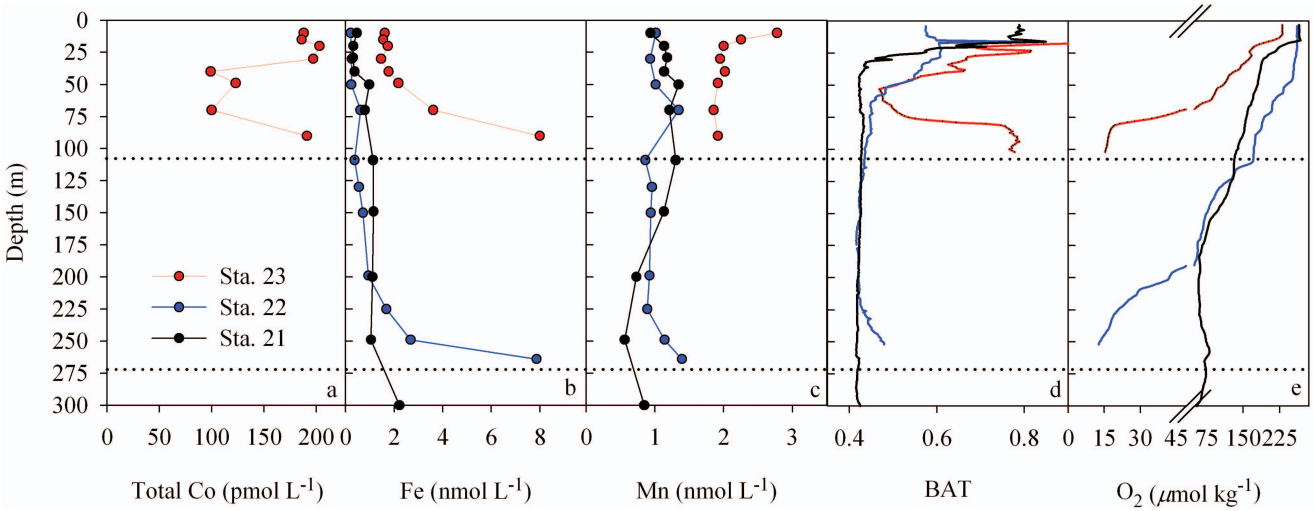

Fig. 11. Vertical profiles of three stations sampled along the Namibian coast. Beam attenuation coefficient (BAT), a proxy for particulate material, increased near the deepest depths sampled for metals. Horizontal dotted lines indicate the bottom depth for the corresponding stations. The lowest oxygen concentration was observed coincident with the high beam attenuation and a marked increase in iron and cobalt concentrations, supporting the notion of a sedimentary source for the metals. (Note, only Sta. 23 is available for total dissolved cobalt due to methodological interferences in these productive coastal waters.)

particulate material on the dissolved inventory of other bioactive metals has been less studied (Johnson et al. 1992; Chase et al. 2005), but may also be significant (Lamborg et al. 2008). Turbidity and particulate metal concentration measurements from the CoFeMUG cruise suggest that this release mechanism may be important for the inventories of these metals, with potential implications for the dissolved iron concentrations, though less so for dissolved manganese and least of all for dissolved cobalt. A significant increase in dissolved iron concentration corresponds with an increase in particulate iron at Sta. 19 that is 7 times higher than the dissolved iron (Fig. 6). Cobalt dissolved and particulate concentrations also increase at the bottom sampled depths (Fig. 6f), but the particulate cobalt concentration is only a small fraction (1/20th) of the dissolved cobalt concentration and a similar trend is observed for manganese (pMn ~ 1/10th of the dMn) (Fig. 6h). These differences in phase partitioning suggest that while the dissolved flux from the sediments may be more important than the particulate flux for cobalt and manganese, this may not be the case for iron. Cycling between the dissolved and particulate phase at the sediment–water interface can support a flux of iron to the water column if a fraction of the dissolved pool is bound by ligands before re-precipitation, as has been observed in the shelf waters along the coast of Oregon and Washington State (Lohan and Bruland 2008). While similar processes may exist for cobalt and manganese cycling, the higher water column dissolved concentrations do not support this as a dominant cobalt or manganese source here. Farther south, sampling at coastal Sta. 21, 22, and 23 approached or penetrated the benthic bottom layer where an increase in total dissolved cobalt and iron concentrations, and to a lesser extent, manganese were observed (Fig. 11). The beam attenuation coefficient, a proxy for sediment and/or particle resuspension (Lam and Bishop 2008), also increased with depth near the bottom of the water column, and oxygen concentrations plummeted (Fig. 11). Given the nearby observation of high particulate iron and low particulate cobalt and manganese at Sta. 19 (Fig. 6), the elevated dissolved iron here was likely derived from a combination of reductive dissolution and particulate fluxes, but the cobalt concentrations were likely primarily derived from reductive dissolution. The smaller manganese trend may be a function of the high concentrations of manganese observed in surface waters (*see* above), masking a sedimentary signal in these shallow waters.

Broad continental shelf environments can enhance metal fluxes by providing more sedimentary surface area from which reduced metals and resuspended particles may be released (Bruland et al. 2005). Consistent with this, the concentration of dissolved iron at depth along the narrow shelf abutting the main transect was high (~ 10-km shelf width, 3 nmol L^{-1} Fe), but the highest concentration of iron was found at depth farther south along the broad shelf (Sta. 23 ~ 150-km shelf width, 8 nmol L^{-1}). Yet, the high iron concentrations found at this southern coastal station decreased immediately to the west (Fig. 1), likely reflecting the differences in physical processes between regions (Fig. 5a,c,d,f,g,i; Table 2). Consistent with this, there is a strong oxygen gradient heading westward from Sta. 23 (Figs. 2, 5c). To the north, oxygen is depleted (as low as 18 μmol kg^{-1} at Sta. 17, 300 m), and the gradual oxygen gradient observed is consistent with offshore advection (Figs. 2, 5a). Our results follow the trend of wide shelves being important iron sources (Table 3); however, they also suggest that low oxygen concentrations and physical processes also contribute to the effective transport of these dissolved metals to the open ocean.

Consideration of aeolian and riverine sources—Both modeled dust deposition studies (Fig. 8a; Mahowald et al. 2005), and low surface dissolved aluminum concentrations are consistent with relatively low aeolian input to this region. Aluminum is a scavenged-type trace element with a

Table 2. Comparison of chemical properties at 400-m depth to surface productivity for two stations from the main transect and one station from the southern transect. Differences in Moderate Resolution Imaging Spectroradiometer (MODIS) Chl *a* concentrations do not mirror differences in trace metals, suggesting that vertical and lateral inputs likely work together to create the observed plumes. Chl *a* concentrations are estimated from an image of MODIS satellite data for a 4-km-resolution average for November 2007 (http://oceancolor.gsfc.nasa.gov/) and average primary productivity (PP) values are from Seawifs December 2007 averaged data (http://oceanwatch.pfeg.noaa.gov/).

Sta.	Surface Chl *a* (mg m^{-3})	Average PP (mg C m^{-2} d^{-1})	Distance to land (km)	O_2 (μmol kg^{-1})	Co (pmol L^{-1})	Fe (nmol L^{-1})	Mn (nmol L^{-1})
13	0.2–0.5	424	1300	42	130	0.71	0.43
17	0.8–1.00	831	275	21	146	0.96	0.78
25	0.8–1.00	860	290	163	42	0.68	0.41

surface-water residence time of $\sim$ 5 yr (Jickells et al. 1994). The open-ocean surface-water concentrations have been used to estimate aeolian deposition using the Model of Aluminum for Dust Calculation in Ocean Waters (MADCOW) model, yielding values that represent an $\sim$ 5-yr running mean of dust deposition and that agree reasonably well with independent estimates over a large range of dust depositions (Measures and Vink 2000). Previous studies of surface aluminum concentrations in the Atlantic show a significant range of concentrations that were higher near the Brazilian coast, lower in the Benguela Upwelling, and highest off the Sahara Desert (Measures 1995; Measures et al. 2008). In the eastern Atlantic, close to our Sta. 13, Measures (1995) showed that there is a very strong north–south gradient in aluminum concentrations from $\sim$ 12 nmol L^{-1} at 15°S to $<$ 2 nmol L^{-1} at 16°S, which was attributed to the convergence of the Angola Current and Benguela Current in the Angola Benguela Frontal Zone. These observations all suggest that while aeolian input is high in the Western Atlantic and the North East Atlantic, dust inputs are generally low in the South East Atlantic.

Surface samples of dissolved aluminum from CoFeMUG are consistent with previous observations (Fig. 8b). Aluminum concentrations imply dust depositions that are at a maximum of 9.4 mg m^{-2} d^{-1} at Sta. 11 and range from 5.7 to 7.67 mg m^{-2} d^{-1} to the west. East of Sta. 11, dust deposition values drop rapidly to 1–3 mg m^{-2} d^{-1}, with the lowest values $<$ 1 mg m^{-2} d^{-1} observed along the coast and the southern transect. It should be noted, however, that in upwelling regions the assumptions of a steady-state surface-water layer are incorrect and thus the MADCOW model will underpredict aeolian deposition (Kaupp et al. 2011). Aluminum concentrations were highest at Sta. 11, and concentrations ranged from 26 to 35 nmol L^{-1} to the west. East of Sta. 11, aluminum concentrations decreased, with the lowest concentrations observed along the coast and in the southern transect (0.7 nmol L^{-1} to 7 nmol L^{-1}; Fig 8b). In contrast, cobalt surface concentrations increased from 24 pmol L^{-1} at Sta. 11 to 184 pmol L^{-1} at Sta. 19. These opposite trends provide evidence that dust was not a primary contributor to the cobalt signals observed in the main transect. While aluminum concentrations are historically high just north of our sampled stations, there was little aeolian contribution during our cruise and at these latitudes. These observations are consistent with results from the Atlantic Meridional Transect expeditions, which also found elevated iron and cobalt but decreased aluminum within the Benguela Upwelling relative to the gyre (Bowie et al. 2002).

We can derive an estimate of potential cobalt input from dust in this region from dissolved aluminum concentrations and dust deposition models. If the composition of dust entering the South Atlantic is similar to the composition of the upper crust (Co : Mn : Fe = 1 : 60 : 3500 from Taylor and McLennan 1985), the input of cobalt and manganese would be small relative to iron. Additionally, recent results suggest that the solubility of cobalt in dust may be quite low (0.14% for natural dust and 0.78% for anthropogenic dust; Thuroczy et al. 2010), though some evidence shows that surface cobalt may display evidence of episodic aeolian input, for instance, in the Sargasso Sea (Shelley et al. 2010). Using

Table 3. Comparison of shelf width and iron concentration in upwelling regions. nd, no data available; PP, primary productivity; SE, southeast.

Study	Location	Shelf width	Lowest [O_2] reported	Fe species	[Fe] nmol L^{-1}	Depth range
Chase et al. 2005	California coast	2.5 km	50–100 μmol L^{-1}	$<$20 μm Fe(III)	0.6	Upwelled waters
					nd	Bottom
Chase et al. 2005	California coast	10 km	50–100 μmol L^{-1}	$<$20 μm Fe(III)	20 Dec	Upwelled waters
					nd	Bottom
Bruland et al. 2005	Peruvian coast	10 km	$<$5 μmol L^{-1}	$<$0.4 μm FeTd*	0.1–0.2	Upwelled waters
					1.4–4.3	Bottom
Bruland et al. 2005	Peruvian coast	150 km	$<$5 μmol L^{-1}	$<$0.4 μm FeTd	3.5–16	Upwelled waters
					48–51	Bottom
This study	SE Atlantic Sta. 19	10 km	35 μmol L^{-1}	$<$0.4 μm FeTd	1	10 m
					3	Bottom
This study	SE Atlantic Sta. 23	150 km	11 μmol L^{-1}	$<$0.4 μm FeTd	1.6	10 m
					8	Bottom

* Td, total dissolved.

this solubility range, a dust input of 0.5 mg m^{-2} d^{-1} (from Fig. 8a, Mahowald et al. 2005, and from deposition estimates using our surface aluminum data Fig. 8b), and a mixed-layer depth of 20 m estimated from temperature gradients (Fig. 5g), aeolian input would contribute only 0.002–0.012 pmol Co L^{-1} yr^{-1} to the eastern end of the basin. This amount would be $< 1\%$ of the total cobalt observed, with a conservative assumption of a cobalt surface-water concentration of 10 pmol L^{-1}, and an estimated surface ocean residence time of < 7.6 yr (Saito and Moffett 2002). Even if cobalt solubility were significantly higher, this source would still remain a minor contributor in this location.

The Congo River empties to the eastern South Atlantic Basin at 6°S, 12°E. Inland from the Congo River, the African Copper Belt (12°S, 26°E) previously produced 40% of the world's cobalt through mining (Prasad 1989). If high cobalt containing dust reached the Congo River and was carried to the coast, this could contribute to the elevated cobalt observed relative to other metals, although we are unaware of any published Congo River cobalt data. Riverine removal rates of manganese and iron due to flocculation have been observed to be 5–10 times faster than that of cobalt (Sholkovitz 1976), which might enhance cobalt abundances relative to iron and manganese. Salinity and temperature signatures are good indications of surface-water source and intrusion of waters from the Angolan Current are characterized by temperatures above 21°C and salinities above 35.9 (John et al. 2004). Based on these criteria, some intrusion of the Angolan Current is observed at Sta. 17 and 18 within the Angola Dome, but the highest surface cobalt concentrations are found at Sta. 19, which has temperature and salinity signatures of the Benguela Coastal Current. This suggests that upwelling along the coast may be a stronger source of cobalt than riverine input. Given the available evidence, aeolian and riverine sources do not appear to be major contributors to the subsurface metal plumes observed in this study, relative to the sedimentary sources discussed above.

Vertical and lateral metal fluxes to the South Atlantic Basin—Metals from the coastal sediments can make their way into the open ocean by both lateral and vertical input vectors. The vertical introduction of these metals occurs primarily via remineralization of sinking organic and inorganic particulate material. Combining dissolved metal data with sediment trap and particulate metal data is useful in considering the influence of vertical and lateral processes on the metal distributions, and similar collections of data have proven useful in understanding the biogeochemistries of manganese and iron (Landing and Bruland 1987; Johnson et al. 1996, 1997). Sediment trap data provide an estimate of the vertical fluxes of exported material delivered to intermediate depths, albeit with some potential bias (Lamborg et al. 2008). Comparison of the particulate metal to dissolved metal concentrations can be informative of potential for transformations between phases, and we observe two overriding trends. First, dissolved and particulate cobalt, iron, and manganese showed parallel trends with depth at the coast (Sta. 19, Fig. 6f–h), suggesting that their sources are related and (or) that there is interaction between phases. Second, in all cases but that of iron, the relative concentrations of the particulate material were orders of magnitude lower than that of the dissolved counterpart (*see* Results section for ratios, Fig. 6). These large differences indicate that if the existing inventory of pP, pCo, and pMn were dissolved or remineralized, they would not contribute significantly to the inventory of dPO_4^{3-}, dCo, and dMn in the water column. This highlights the likely shorter residence times of these particulate metals relative to their dissolved phases. In the following paragraphs, we compare the dissolved, particulate, and sediment trap metal data from a coastal station (Sta. 19) to an open-ocean station (Sta. 13).

At the open-ocean Sta. 13, convex vertical profile structure was observed for dissolved cobalt, iron, and phosphorus, consistent with input via remineralization and the diffusion of metals from below (Sta. 13, Fig. 6a–c). Particulate profiles at this station exhibit surface particle maxima for cobalt and phosphorus, consistent with uptake and remineralization; however, this trend was not observed in the particulate iron and manganese profiles. Sediment trap data provide an estimate of remineralization rates, showing a decrease in flux with depth between the 60-m and 150-m traps (Fig. 7b–e). As described in the Results, the integrated metal fluxes due to remineralization delivered 0.013 pmol Co L^{-1} d^{-1}, 8.5 pmol Fe L^{-1} d^{-1}, 0.11 pmol Mn L^{-1} d^{-1}, and 11.2 nmol P L^{-1} d^{-1} to the water column between these sediment trap depths (Sta. 13). Enhanced primary productivity was observed over the region with the subsurface metal plumes (http://las.pfeg.noaa.gov/; Fig. 8c). In addition to these observations, there is a strong linear relationship between cobalt and phosphate along the 27.0–27.1 density layer (data not shown, $n = 13$, $r^2 = 0.85$, slope = 151, μmol Co : mol PO_4^{3-}), suggesting that timescales of removal of cobalt are slow, and reflect an integrated biological remineralization signal similar to that of PO_4^{3-}. These three lines of evidence support the influence of remineralization on water column distributions, and are consistent with the cobalt plume being influenced by lateral gradients in vertical fluxes of dissolved cobalt, as has been argued for manganese in observations and models of manganese distributions in the Pacific and Atlantic (Johnson et al. 1996).

There has been a debate in the literature regarding the relative importance of lateral from sedimentary sources (Landing and Bruland 1987; Martin et al. 1989) vs. vertical fluxes (and lateral gradients of those vertical fluxes) without the need to invoke sedimentary sources (Johnson et al. 1996, 1997) for the hybrid-type metals iron and manganese. In the case of the South Atlantic plumes we document here, we believe both processes are contributing to the cobalt plume formation, with the former described above and the latter sedimentary flux based on the four observations: (1) previous documentation of cobalt sediment fluxes from anoxic coastal environments (Heggie and Lewis 1984), (2) presence of seasonal anoxia along the Namibian coastal shelf (Bruchert et al. 2003; Mohrholz et al. 2008), (3) low surface-water cobalt inventory, and (4) low atmospheric sources in this region. Future modeling studies could examine these two processes (focusing on sources and initial/boundary conditions), as well as the influence of continuing ocean deoxygenation on hybrid-type metal basin inventories.

Along the coast (Sta. 19, Fig. 6), localized processes that control the dissolved and particulate trace metal distributions are more complex, and both surface- and bottom-water maxima are observed in the particulate profiles of cobalt, manganese, and phosphorus (Fig. 6e,f,h). Consistent with the degradation of sinking particulate organic matter, shallow maxima are observed in the dissolved cobalt, iron, manganese, and phosphorus profiles, coincident with a local oxygen minimum (Fig. 5a, 6f–h). The 60-m flux along the coast was indistinguishable from the open-ocean flux within the error of the measurement, and the sediment trap data did not detect remineralization for iron, manganese, and phosphorus (Sta. 19, Fig. 7b,d,e), likely due to other particulate cycling processes such as the preservation of sinking particulate matter due to high productivity and low oxygen and/or lateral advection of resuspended particulate matter. Total mass flux at 150 m was larger than that at 60 m, with no noticeable change in the iron, manganese, and phosphorus fluxes (Fig. 7a,b), which supports this possible influence of particulate cycling processes other than remineralization. Table 2 shows some values of interest at Sta. 13, Sta. 19, and Sta. 25, off the coast in the southern transect. While average chlorophyll *a* (Chl *a*) concentrations and primary production estimated from satellite data (http://oceancolor.gsfc.nasa.gov/, http://las.pfeg.noaa.gov/) are quite similar at Sta. 17 and 25, their respective subsurface metal and oxygen signals are different. Additionally, the iron and manganese concentrations at Sta. 13 are quite similar to that of Sta. 25, even though primary productivity and Chl *a* concentrations are twice as high. This again highlights the different physical processes influencing the northern and southern transects and suggests that the subsurface metal plumes are likely generated by the confluence of vertical and lateral processes that are not easily separated.

The particulate trace metal profiles for iron and manganese at the open-ocean Sta. 13 also show steady increases in concentration from the surface to 600 m (Fig. 6c,d), and the particulate concentrations were respectively 140- and 6-fold less than the respective coastal particulate concentrations, consistent with a loss of particulate iron and manganese with water movement westward (P. Lam and D. Ohnemus unpubl.; Fig. 6c,d,g,h). The changes in concentration of particulate and dissolved metals can also be compared between the open ocean and coastal region, assuming lateral advection contributes to transporting a fraction of both phases westward within the OMZ from Sta. 19 to Sta. 13. Calculated as the average decrease in concentration for each species between 300- and 400-m depth from Sta. 19 to Sta. 13, particulate iron decreased 28 times faster than dissolved iron (Fig. 6c,g), particulate cobalt decreased 7 times faster than dissolved cobalt (Fig. 6b,f), and particulate manganese decreased 2 times faster than dissolved manganese (Fig. 6d,f,h). This could also be evidence of decreased productivity and/or export. Low particulate cobalt concentrations at intermediate depths suggest that the scavenging of the laterally advected dissolved cobalt occurs slowly enough that it does not imprint a signal on the vertical profile of particulate cobalt (Figs. 6b, 7c), and this is supported by the observed persistence of enhanced dissolved concentrations into the center of the South Atlantic basin and the linear relationships with dissolved oxygen and nitrous oxide (Figs. 4, 9). While these simultaneous dissolved, particulate, and sediment trap data provide an intriguing picture of the complex coastal and open-ocean environments, future process studies are needed to better characterize the interactions between phases and processes.

Shallow coastal cobalt plume—The high surface concentrations of cobalt (151–200 pmol L^{-1} in the upper 60 m, Fig. 4) observed near the coast in the main transect are likely associated with the upwelling of waters high in reduced metals. Oxygen concentrations drop below 100 μmol kg^{-1} at 15-m depth and reach as low as 29 μmol kg^{-1} in the upper 60 m. This high cobalt signal is coincident with strong beam attenuation likely due to high biological productivity (data not shown) and high nitrogen fixation activity (Sohm et al. 2011). Thermocline nitrate $\delta^{15}N$ values also decrease to the east and correlate with cobalt (data not shown, $r^2 = 0.70$), which would be consistent with an input of low $\delta^{15}N$ material from nitrogen fixation (Casciotti et al. 2008), although other processes may contribute to this pattern. While cobalt is known to be a required micronutrient in the marine cyanobacteria (Saito et al. 2005), cobalt requirements in nitrogen-fixing marine diazotrophs have not been well characterized, and it is possible that the abundant cobalt and iron contribute to the nitrogen fixation measured in this region. Surface concentrations of iron are also elevated along the coast, though not to the same extent, which might be due to increased biological uptake. Surface concentrations of dissolved manganese were not significantly elevated relative to westward stations, though a source in this region could be masked by the pervasively high surface concentrations observed across the basin.

This paper highlights the advantages of the sectional approach to trace metal distribution studies being deployed in the GEOTRACES program, where the influence of important processes are more readily apparent in a section relative to vertical profiles. Specifically, we observed the eastern African boundary of the Southern Atlantic to be a strong source of cobalt. Iron and manganese were also elevated near the coast, but their concentrations rapidly decreased with distance from shore, likely due to faster oxidation and (or) scavenging kinetics of these metals in this environment. The coastal source identified here is important because cobalt, iron, and manganese have relatively small oceanic inventories, and perturbations in their concentrations can create large gradients, significantly affecting their cycling and subsequent roles as important micronutrients to oceanic phytoplankton. Relationships between metals, low oxygen, and high beam attenuation in bottom waters near the coast suggest that reductive dissolution and particle resuspension were the major sources of the elevated metal concentrations observed. Dissolved oxygen concentration and shelf size influenced the magnitude of the coastal metal source fluxes, while the delivery of these metals to the ocean interior was dependent upon the physical processes influencing the system (wind-driven upwelling, advection, and slow ventilation), the extent to which each element was susceptible to scavenging,

and the biological processes that deliver metals exported from the surface through uptake and remineralization. With the observed and predicted expansion of low-oxygen regions in oceanic and coastal marine environments globally (Stramma et al. 2008), the fluxes of iron, cobalt, and manganese will also likely increase in magnitude in OMZs, with potentially important implications for ocean primary productivity and nitrogen fixation.

Acknowledgments

We thank Gabrielle Rocap, Chad Hammerschmidt, Alysia Cox, Marian Westley, Mike Sieracki, and Eric Webb for assistance during the cruise, Erin Bertrand and Ed Sholkovitz for helpful conversations, and Ken Johnson and an anonymous reviewer for useful comments. We are particularly indebted to the captain and crew of the R/V *Knorr:* without their exceptional support, this ocean section would not have been possible. We thank Natalie Mahowald for generously letting us use her dust deposition model (Mahowald et al. 2005). We also thank Scot Birdwhistell in the Woods Hole Oceanographic Institution (WHOI) ICP-MS facility. We also thank the GEOTRACES community and intercalibration program. We thank the nations of Angola and Namibia for providing research clearance in their exclusive economic zones. We are grateful to Christa Pohl for sharing previous Benguela cruise results and dedicate this manuscript to her memory. This research was supported US National Science Foundation Chemical Oceanography (Division of Ocean Sciences OCE-0452883, OCE-0752291, OCE-0928414, OCE-1031271), the Center for Microbial Research and Education, the Gordon and Betty Moore Foundation, the WHOI Coastal Ocean Institute, and the WHOI Ocean Life Institute.

References

Armstrong, F. A. J., C. R. Stearns, and J. D. H. Strickland. 1967. The measurement of upwelling and subsequent biological process by means of the Technicon Autoanalyzer Æ and associated equipment. Deep-Sea Res. **14:** 381–389.

Atlas, E. L., S. W. Hager, L. I. Gordon, and P. K. Park. 1971. A practical manual for use of the Technicon Autoanalyzer ™ in seawater nutrient analyses; revised. Technical Report 215. Oregon State Univ., Department of Oceanography, Reference No. 71-22.

Bernhardt, H., and A. Wilhelms. 1967. The continuous determination of low level iron, soluble phosphate and total phosphate with the AutoAnalyzer™, p. 386. 1967. Technicon Symposium, 1967, v. 1. Technicon Instruments Corporation, Chauncey, New York.

Bertrand, E. M., M. A. Saito, J. M. Rose, C. R. Riesselman, M. C. Lohan, A. E. Noble, P. A. Lee, and G. R. DiTullio. 2007. Vitamin B_{12} and iron co-limitation of phytoplankton growth in the Ross Sea. Limnol. Oceanogr. **52:** 1079–1093, doi:10.4319/lo.2007.52.3.1079

Bowie, A. R., D. J. Whitworth, E. P. Achterberg, R. Fauzi, C. Mantoura, and P. J. Worsfold. 2002. Biogeochemistry of Fe and other trace elements (Al, Co, Ni) in the upper Atlantic Ocean. Deep-Sea Res. I **49:** 605–636, doi:10.1016/S0967-0637(01)00061-9

Bruchert, V., B. B. Jorgensen, K. Neumann, D. Riechmann, M. Schlosser, and H. Schulz. 2003. Regulation of bacterial sulfate reduction and hydrogen sulfide fluxes in the central Namibian coastal upwelling zone. Geochim. Cosmochim. Acta **67:** 4505–4518, doi:10.1016/S0016-7037(03)00275-8

Bruland, K., K. Orians, and J. Cowen. 1994. Reactive trace metals in the stratified central North Pacific. Geochim. Cosmochim. Acta **58:** 3171–3182, doi:10.1016/0016-7037(94)90044-2

Bruland, K. W. 2010. GEOTRACES co intercalibration results [Internet]. Copyright GEOTRACES 2012, Available from http://www.geotraces.org/images/stories/documents/intercalibration/Files/Reference_Samples_November11/SAFe_Ref_Co.pdf

———, and M. C. Lohan. 2003. Controls of trace metals in seawater, p. 23–47. *In* H. D. Holland and K. K. Turekian [eds.], Treatise on geochemistry, v. 6. Elsevier.

———, E. L. Rue, G. J. Smith, and G. R. DiTullio. 2005. Iron, macronutrients and diatom blooms in the Peru Upwelling regime: Brown and blue waters of Peru. Mar. Chem. **93:** 81–103, doi:10.1016/j.marchem.2004.06.011

Casciotti, K. L., T. W. Trull, D. M. Glover, and D. Davies. 2008. Constraints on nitrogen cycling at the subtropical North Pacific Station ALOHA from isotopic measurements of nitrate and particulate nitrogen. Deep-Sea Res. II **55:** 1661–1672, doi:10.1016/j.dsr2.2008.04.017

Chase, Z., K. S. Johnson, V. A. Elrod, J. N. Plant, S. E. Fitzwater, L. Pickell, and C. M. Sakamoto. 2005. Manganese and iron distributions off central California influenced by upwelling and shelf width. Mar. Chem. **95:** 235–254, doi:10.1016/j.marchem.2004.09.006

Dyrssen, D., and K. Kremling. 1990. Increasing hydrogen sulfide concentration and trace metal behavior in the anoxic Baltic waters. Mar. Chem. **30:** 193–204, doi:10.1016/0304-4203(90)90070-S

Elrod, V. A., W. M. Berelson, K. H. Coale, and K. Johnson. 2004. The flux of iron from continental shelf sediments: A missing source for global budgets. Geophys. Res. Lett. **31:** L12307, doi:10.1029/2004GL020216

Emeis, K.-C., V. Bruchert, B. Currie, R. Endlier, T. Ferdelman, A. Kiessling, T. Leipe, K. Noli-Peard, U. Struck, and T. Vogt. 2004. Shallow gas in shelf sediments of the Namibian coastal upwelling ecosystem. Cont. Shelf Res. **24:** 627–642, doi:10.1016/j.csr.2004.01.007

Gordon, L. I., J. C. Jennings, Jr, A. A. Ross, and J. M. Krest. 1994. A suggested protocol for continuous flow analysis of seawater nutrients (phosphate, nitrate, nitrite, and silicic acid) in the WOCE Hydrographic Program and the Joint Global Ocean Fluxes Study. WHP Office Report 91-1. Revision 1, Nov. 1994. WOCE Hydrographic Program Office, Woods Hole, MA.

Heggie, D., and T. Lewis. 1984. Cobalt in pore waters of marine sediments. Nature **311:** 453–455, doi:10.1038/311453a0

Jickells, T., T. Church, A. Veron, and R. Arimoto. 1994. Atmospheric inputs of manganese and aluminum to the Sargasso Sea and their relation to surface water concentrations. Mar. Chem. **46:** 283–292, doi:10.1016/0304-4203(94)90083-3

John, H.-Ch., V. Mohrholz, J. R. E. Lutjeharms, S. Weeks, R. Cloete, A. Kreiner, and D. da Silva Neto. 2004. Oceanographic and faunistic structures across an Angola Current intrusion into northern Namibian waters. J. Mar. Syst. **46:** 1–22, doi:10.1016/j.jmarsys.2003.11.021

Johnson, K. S., W. M. Berelson, K. H. Coale, T. L. Coley, V. A. Elrod, W. R. Fairey, H. D. Iams, T. E. Kilgore, and J. L. Nowicki. 1992. Manganese flux from continental margin sediments in a transect through the oxygen minimum. Science **257:** 1242–1245, doi:10.1126/science.257.5074.1242

———, E. A. Boyle, K. Bruland, K. Coale, C. Measures, J. Moffett, A. Aguilar-Islas, K. Barbeau, B. Bergquist, A. Bowie, K. Buck, Y. Cai, Z. Chase, J. Cullen, T. Doi, V. Elrod, S. Fitzwater, M. Gordon, A. King, P. Laan, L. Laglera-Baquer, W. Landing, M. Lohan, J. Mendez, A. Milne, H. Obata, L. Ossiander, J. Plant, G. Sarthou, P.

Sedwick, G. J. Smith, B. Sohst, S. Tanner, S. Van den Berg, and J. Wu. 2007. Developing iron standards for seawater. EOS Trans. **88:** 11, 131–132, doi:10.1029/2007EO110003

———, K. H. Coale, W. M. Berelson, and R. M. Gordon. 1996. On the formation of the manganese maximum in the oxygen minimum. Geochim. Cosmochim. Acta **60:** 1291–1299, doi:10.1016/0016-7037(96)00005-1

———, R. M. Gordon, and K. H. Coale. 1997. What controls dissolved iron in the world ocean? Mar. Chem. **57:** 137–161, doi:10.1016/S0304-4203(97)00043-1

———, P. M. Stout, W. M. Berelson, and C. M. Sakamoto-Arnold. 1988. Cobalt and copper distributions in the waters of Santa Monica Basin, California. Nature **332:** 527–530, doi:10.1038/332527a0

Kaupp, L., C. I. Measures, K. E. Selph, and F. T. Mackenzie. 2011. The distribution of dissolved Fe and Al in the upper waters of the eastern Equatorial Pacific. Deep-Sea Res. II **58:** 296–310, doi:10.1016/j.dsr2.2010.08.009

Klinkhammer, G. P. 1980. Observations of the distribution of manganese over the East Pacific Rise. Chem. Geol. **29:** 211–226, doi:10.1016/0009-2541(80)90021-2

Kostianoy, A. G., and J. R. E. Lutjeharms. 1999. Atmospheric effects in the Angola–Benguela frontal zone. J. Geophys. Res. **104:** 20962–20970, doi:10.1029/1999JC900017

Lam, P. J., and J. K. B. Bishop. 2008. The continental margin is a key source of iron to the HNLC North Pacific Ocean. Geophys. Res. Lett. **35:** L07608, doi:10.1029/2008GL033294

———, ———, C. C. Henning, M. A. Marcus, G. A. Waychunas, and I. Y. Fung. 2006. Wintertime phytoplankton bloom in the subarctic Pacific supported by continental margin iron. Global Biogeochem. Cycles **20:** GB1006, doi:10.1029/2005GB002557

Lamborg, C. H., K. O. Buesseler, and P. J. Lam. 2008. Sinking fluxes of minor and trace elements in the North Pacific Ocean measured during the VERTIGO program. Deep-Sea Res. II **55:** 1564–1577, doi:10.1016/j.dsr2.2008.04.012

Landing, W. M., and K. W. Bruland. 1987. The contrasting biogeochemistry of iron and manganese in the Pacific Ocean. Geochim. Cosmochim. Acta **51:** 29–43, doi:10.1016/0016-7037(87)90004-4

Lass, H. U., and V. Mohrholz. 2008. On the interaction between the subtropical gyre and the Subtropical Cell on the shelf of the SE Atlantic. J. Mar. Syst. **74:** 1–43, doi:10.1016/j.jmarsys.2007.09.008

Lavik, G., T. Stuhrmann, V. Bruchert, A. Van der Plas, V. Mohrholz, P. Lam, M. Muβmann, B. M. Fuchs, R. Amann, U. Lass, and M. M. M. Kuypers. 2009. Detoxification of suphidic African shelf waters by blooming chemolithotrophs. Nature **457:** 581–585, doi:10.1038/nature07588

Lohan, M. C., and K. W. Bruland. 2008. Elevated Fe(II) and dissolved Fe in hypoxic shelf waters off Oregon and Washington: An enhanced source of iron to coastal upwelling regimes. Environ. Sci. Technol. **42:** 6462–6468, doi:10.1021/es800144j

Mahowald, N. M., A. R. Baker, G. Bergametti, N. Brooks, R. A. Duce, T. D. Jickells, N. Kubilay, J. M. Prospero, and I. Tegen. 2005. Atmospheric global dust cycle and iron inputs to the ocean. Global Biogeochem. Cycles **19:** GB4025, doi:10.1029/2004GB002402

Martin, J. H., R. M. Gordon, S. Fitzwater, and W. W. Broenkow. 1989. VERTEX: Phytoplankton/iron studies in the Gulf of Alaska. Deep-Sea Res. **36:** 649–680.

McIlvin, M. R., and K. L. Casciotti. 2010. Fully automated system for stable isotopic analyses of dissolved nitrous oxide at natural abundance levels. Limnol. Oceanogr.: Methods **8:** 54–66, doi:10.4319/lom.2010.8.0054

———, and ———. 2011. Technical updates to the bacterial method for nitrate isotopic analyses. Anal. Chem. **83:** 1850–1856, doi:10.1021/ac1028984

Measures, C. I. 1995. The distributions of Al in the IOC stations of the eastern Atlantic between 30°S and 34°N. Mar. Chem **49:** 267–281, doi:10.1016/0304-4203(95)00017-L

———, W. M. Landing, M. T. Brown, and C. S. Buck. 2008. High-resolution Al and Fe data from the Atlantic Ocean CLIVAR-CO2 Repeat Hydrography A16N transect: Extensive linkages between atmospheric dust and upper ocean geochemistry. Global Biogeochem. Cycles **22:** GB1005, doi:10.1029/2007GB003042

———, and S. Vink. 2000. On the use of dissolved aluminum in surface waters to estimate dust deposition to the ocean. Global Biogeochem. Cycles **14:** 317–327, doi:10.1029/1999GB001188

Moffett, J. W., T. J. Goepfert, and S. W. A. Naqvi. 2007. Reduced iron associated with secondary nitrite maxima in the Arabian Sea. Deep-Sea Res. I **54:** 1341–1349, doi:10.1016/j.dsr.2007.04.004

———, and J. Ho. 1996. Oxidation of cobalt and manganese in seawater via a common microbially catalyzed pathway. Geochim. Cosmochim. Acta **60:** 3415–3424, doi:10.1016/0016-7037(96)00176-7

Mohrholz, V., C. H. Bartholomae, A. K. Van Der Plas, and H. U. Lass. 2008. The seasonal variability of the northern Benguela undercurrent and its relation to the oxygen budget on the shelf. Cont. Shelf Res. **28:** 424–441, doi:10.1016/j.csr.2007.10.001

Moore, C. M., M. M. Mills, E. P. Achterberg, R. J. Geider, J. LaRoche, M. I. Lucas, E. L. McDonagh, X. Pan, A. J. Poulton, M. J. A. Rijkenberg, D. J. Suggett, S. J. Ussher, and E. M. S. Woodward. 2009. Large-scale distribution of Atlantic nitrogen fixation controlled by iron availability. Nature Geosci. **2:** 867–871, doi:10.1038/ngeo667

Moore, J. K., and O. Braucher. 2008. Sedimentary and mineral dust sources of dissolved iron to the World Ocean. Biogeosciences **4:** 1279–1327.

Morel, F. M. M., A. J. Milligan, M. A. Saito, D. H. Heinrich, and K. T. Karl. 2003. Marine bioinorganic chemistry: The role of trace metals in the oceanic cycles of major nutrients, p. 113–143. *In* H. D. Holland and K. K. Turekian [eds.], Treatise on geochemistry, v. 6. Elsevier.

Noble, A. E., M. A. Saito, K. Maiti, and C. Benitez-Nelson. 2008. Cobalt, manganese, and iron near the Hawaiian Islands: A potential concentrating mechanism for cobalt within a cyclonic eddy and implications for the hybrid-type trace metals. Deep-Sea Res. II **55:** 1473–1490, doi:10.1016/j.dsr2.2008.02.010

Panzeca, C., A. J. Beck, K. Leblanc, G. T. Taylor, D. A. Hutchins, and S. A. Sanudo-Wilhelmy. 2008. Potential cobalt limitation of vitamin B_{12} synthesis in the North Atlantic Ocean. Global Biogeochem. Cycles **22:** GB2029, doi:10.1029/2007GB003124

Parker, D. L., T. Morita, M. L. Mozafarzadeh, R. Verity, J. K. McCarthy, and B. M. Tebo. 2007. Inter-relationships of MnO_2 precipitation, siderophore-Mn(III) complex formation, siderophore degradation, and iron limitation in Mn(II)-oxidizing bacterial cultures. Geochim. Cosmochim. Acta **71:** 5672–5683, doi:10.1016/j.gca.2007.03.042

Patton, C. J. 1983. Design, characterization and applications of a miniature continuous flow analysis system. Ph.D. thesis. Michigan State Univ.

Peterson, R. G., and L. Stramma. 1991. Upper-level circulation in the South Atlantic Ocean. Prog. Oceanogr. **26:** 1–73, doi:10.1016/0079-6611(91)90006-8

Pohl, C., P. L. Croot, U. Hennings, T. Daberkow, G. Budeus, and M. R. V. D. Loeff. 2011. Synoptic transects on the distribution of trace elements (Hg, Pb, Cd, Cu, Ni, Zn, Co, Mn, Fe, and Al) in surface waters of the Northern- and Southern East Atlantic. J. Mar. Syst. **84:** 28–41, doi:10.1016/j.jmarsys.2010.08.003

Prasad, M. S. 1989. Production of copper and cobalt at Gecamines, Zaire. Miner. Eng. **2:** 521–541, doi:10.1016/0892-6875(89)90087-3

Reed, D. C., C. P. Slomp, and B. G. Gustafsson. 2011. Sedimentary phosphorus dynamics and the evolution of bottom-water hypoxia: A coupled benthic–pelagic model of a coastal system. Limnol. Oceanogr. **56:** 1075–1092, doi:10.4319/lo.2011.56.3.1075

Saito, M. A., E. M. Bertrand, V. Bulygin, D. Moran, S. Dutkiewicz, F. Monteiro, M. J. Follows, F. W. Valois, and J. B. Waterbury. 2011. Iron conservation by reduction of metalloenzyme inventories in the marine diazotroph *Crocosphaera watsonii*. Proc. Natl. Acad. Sci. USA **108:** 2184–2189, doi:10.1073/pnas.1006943108

———, and T. J. Goepfert. 2008. Zinc-cobalt colimitation in *Phaeocystis antarctica*. Limnol. Oceanogr. **53:** 266–275, doi:10.4319/lo.2008.53.1.0266

———, ———, and J. T. Ritt. 2008. Some thoughts on the concept of colimitation: Three definitions and the importance of bioavailability. Limnol. Oceanogr. **53:** 276–290, doi:10.4319/lo.2008.53.1.0276

———, and J. W. Moffett. 2001. Complexation of cobalt by natural organic ligands in the Sargasso Sea as determined by a new high-sensitivity electrochemical cobalt speciation method suitable for open ocean work. Mar. Chem. **75:** 49–68, doi:10.1016/S0304-4203(01)00025-1

———, and ———. 2002. Temporal and spatial variability of cobalt in the Atlantic Ocean. Geochim. Cosmochim. Acta **66:** 1943–1953, doi:10.1016/S0016-7037(02)00829-3

———, ——— , S. W. Chisholm, and J. B. Waterbury. 2002. Cobalt limitation and uptake in *Prochlorococcus*. Limnol. Oceanogr. **47:** 1629–1636, doi:10.4319/lo.2002.47.6.1629

———, ———, and G. Ditullio. 2004. Cobalt and nickel in the Peru Upwelling region: A major flux of cobalt utilized as a micronutrient. Global Biogeochem. Cycles **18:** GB4030, doi:10.1029/2003GB002216

———, G. Rocap, and J. W. Moffett. 2005. Production of cobalt binding ligands in a *Synechococcus* feature at the Costa Rica Upwelling Dome. Limnol. Oceanogr. **50:** 279–290, doi:10.4319/lo.2005.50.1.0279

———, and D. L. Schneider. 2006. Examination of precipitation chemistry and improvements in precision using the $Mg(OH)_2$ preconcentration ICP-MS method for high-throughput analysis of open-ocean Fe and Mn in seawater. Anal. Chim. Acta **565:** 222–233, doi:10.1016/j.aca.2006.02.028

Schlitzer, R. 2011. Ocean data view, version 4.4.2. [Internet]. Available from http://odv.awi.de

Sharma, V. S., R. B. Pilz, G. R. Boss, and D. Magde. 2003. Reactions of nitric oxide with vitamin B_{12} and its precursor, cobinamide. Biochemistry **42:** 8900–8908, doi:10.1021/bi034469t

Shelley, R. U., B. Zachhuber, P. Sedwick, P. J. Worsfold, and M. C. Lohan. 2010. Determination of total dissolved cobalt in UV-irradiated seawater using flow injection with chemiluminescence detection. Limnol. Oceanogr.: Methods **8:** 352–362, doi:10.4319/lom.2010.8.352

Sholkovitz, E. R. 1976. Flocculation of dissolved organic and inorganic matter during the mixing of river water and seawater. Geochim. Cosmochim. Acta **40:** 831–845, doi:10.1016/0016-7037(76)90035-1

Sohm, J. A., J. A. Hilton, A. E. Noble, J. P. Zehr, M. A. Saito, and E. A. Webb. 2011. Nitrogen fixation in the South Atlantic Gyre and the Benguela Upwelling System. Geophys. Res. Letters. **38:** L16608, doi:10.1029/2011GL048315

Statham, P. J., P. A. Yeats, and W. M. Landing. 1998. Manganese in the eastern Atlantic Ocean: Processes influencing deep and surface water distributions. Mar. Chem. **61:** 55–68, doi:10.1016/S0304-4203(98)00007-3

Steinberg, D. K., C. A. Carlson, N. R. Bates, R. J. Johnson, A. F. Michaels, and A. H. Knapp. 2001. Overview of the US JGOFS Bermuda Atlantic Time-series Study (BATS): A decade-scale look at ocean biology and biogeochemistry. Deep-Sea Res. II **48:** 1405–1448, doi:10.1016/S0967-0645(00)00148-X

Stramma, L., G. C. Johnson, J. Sprintall, and V. Mohrholz. 2008. Expanding oxygen-minimum zones in the tropical oceans. Science **320:** 655–658, doi:10.1126/science.1153847

Sunda, W., and S. A. Huntsman. 1995. Cobalt and zinc interreplacement in marine phytoplankton: Biological and geochemical implications. Limnol. Oceanogr. **40:** 1404–1417, doi:10.4319/lo.1995.40.8.1404

Sunda, W. G., and S. A. Huntsman. 1988. Effect of sunlight on redox cycles of manganese in the southwestern Sargasso Sea. Deep-Sea Res. **35:** 1297–1317.

Taylor, S. R., and S. M. McLennan. 1985. The continental crust: Its composition and evolution. Blackwell Scientific.

Tebo, B., K. Nealson, S. Emerson, and L. Jacobs. 1984. Microbial meditation of Mn(II) and Co(II) precipitation at the O_2/H_2 interfaces in two anoxic fjords. Limnol. Oceanogr. **29:** 1247–1258, doi:10.4319/lo.1984.29.6.1247

Tebo, B. M., J. R. Bargar, B. G. Clement, G. J. Dick, K. J. Murray, D. Parker, R. Verity, and S. M. Webb. 2004. Biogenic manganese oxides: Properties and mechanisms of formation. Annu. Rev. Earth Planet. Sci. **32:** 287–328, doi:10.1146/annurev.earth.32.101802.120213

Thuroczy, C.-E., M. Boye, and R. Losno. 2010. Dissolution of cobalt and zinc from natural and anthropogenic dusts in seawater. Biogeosciences **7:** 1927–1936, doi:10.5194/bg-7-1927-2010

Vink, S., and C. Measures. 2001. The role of dust deposition in determining surface water distributions of Al and Fe in the South West Atlantic. Deep-Sea Res. II **48:** 2787–2809, doi:10.1016/S0967-0645(01)00018-2

Ward, B. B., and O. C. Zafiriou. 1988. Nitrification and nitric oxide in the oxygen minimum of the eastern tropical North Pacific. Deep-Sea Res. **35:** 1127–1142.

Weeks, S. J., and F. A. Shillington. 1994. Interannual scales of variation of pigment concentrations from coastal zone color scanner data in the Benguela Upwelling system and the Subtropical Convergence zone south of Africa. J. Geophys. Res. **99:** 7385–7399, doi:10.1029/93JC02143

Wu, J., W. Sunda, E. A. Boyle, and D. M. Karl. 2000. Phosphate depletion in the Western North Atlantic Ocean. Science **289:** 759–762, doi:10.1126/science.289.5480.759

Yoshida, N. 1988. ^{15}N-depleted N_2O as product of nitrification. Nature **355:** 528–529, doi:10.1038/335528a0

Associate editor: Mary I. Scranton

Received: 09 February 2011
Accepted: 20 October 2011
Amended: 10 February 2012